FEATURE ARTICLE

Nanostructured copper oxide semiconductors: a perspective on materials, synthesis methods and applications

Ahmad Sabirin Zoolfakar,[*ab] Rozina Abdul Rani,[a] Anthony J. Morfa,[c] Anthony P. O'Mullane[d] and Kourosh Kalantar-zadeh[*a]

The oxides of copper (Cu_xO) are fascinating materials due to their remarkable optical, electrical, thermal and magnetic properties. Nanostructuring of Cu_xO can further enhance the performance of this important functional material and provide it with unique properties that do not exist in its bulk form. Three distinctly different phases of Cu_xO, mainly CuO, Cu_2O and Cu_4O_3, can be prepared by numerous synthesis techniques including, vapour deposition and liquid phase chemical methods. In this article, we present a review of nanostructured Cu_xO focusing on their material properties, methods of synthesis and an overview of various applications that have been associated with nanostructured Cu_xO.

[a]*School of Electrical and Computer Engineering, RMIT University, Melbourne, VIC 3001, Australia. E-mail: kourosh.kalantar@rmit.edu.au*

[b]*Faculty of Electrical Engineering, Universiti Teknologi MARA, 40450 Shah Alam, Malaysia. E-mail: ahmad074@salam.uitm.edu.my*

[c]*Freie Universität Berlin, Fachbereich Physik, 14195 Berlin, Germany*

[d]*School of Chemistry, Physics and Mechanical Engineering, Queensland University of Technology, GPO Box 2434, Brisbane, QLD, 4001, Australia*

1. Introduction

Lately, there has been a great deal of interest in nanostructured copper oxide (Cu_xO) semiconductors. This interest in nanostructured Cu_xO is fuelled due to their remarkable physical and chemical properties as well as exciting prospects for a variety of applications.[1,2]

Nanostructured copper oxides are relatively abundant in nature,[3] and a wide range of information is now available for their synthesis. Nanostructured Cu_xO can be grown using different synthesis techniques, including vapour and liquid phase deposition processes, in which a variety of nano-morphologies can be obtained.

Nanostructured copper oxides are exceptionally versatile and offer unique characteristics in many applications. Cu_xO nanomaterials have been used as colouring agents for the production of Roman mosaic glasses and antique ceramics for thousands of years.[4,5] Nanosized Cu_xO has been widely utilized as a fungicide[6,7] and in anti-fouling paints[8,9] due to its biocidal capability. With the advent of nanotechnology, Cu_xO has shown a great impact in numerous research fields including optics,

Ahmad Sabirin Zoolfakar received his B. Eng. (Electrical) with Honours from Universiti Malaya, Malaysia (2001), M. Sc. (Microelectronic Systems and Telecommunications) from The University of Liverpool, United Kingdom (2003) and Ph.D at RMIT University, Australia (2014). He is a senior lecturer in the Faculty of Electrical Engineering at Universiti Teknologi MARA. His research interests include aqueous chemical synthesis, gas vapour synthesis, nanotechnology and materials science. At present the prime focus of his work concerns metal oxide for application in sensor development.

Rozina Abdul Rani received her Bachelor of Engineering (Electrical and Electronic) with Honours (2001) and Master of Science (2007) degree from Universiti Sains Malaysia, Malaysia. She is currently undertaking her candidature for a Ph.D at RMIT University. Her research interests include synthesis and characterization of nanostructured metal oxides, dye-sensitized solar cells, chemical sensors and batteries.

sensors, tribology, superconductors, electrochemistry and electronics.[10–14]

The most common crystal phases of Cu_xO are: (a) CuO also known as copper(II) oxide or cupric oxide where the mineral is known as tenorite, (b) Cu_2O also known as copper(I) oxide or cuprous oxide with the mineral name of cuprite, and (c) Cu_4O_3 with the mineral name of paramelaconite.[1,2,15,16]

In this feature article, we present a general, yet complete, review of nanostructured Cu_xO. The present review is distinguishable from other reviews,[1,17] which have a focus on one type of Cu_xO (generally CuO or Cu_2O), while this review endeavors to thoroughly discuss three types of Cu_xO, including CuO, Cu_2O and Cu_4O_3. The organization of this review is as follows: firstly, we discuss the fundamental chemical and physical properties of nanostructured Cu_xO and then we summarize the different methods of synthesis that have been reported. Finally we present a selection of interesting applications that exploit Cu_xO and illustrate the enhancements made possible by using the nanostructured form of this material.

2. Fundamental properties

In this section, the fundamental properties such as crystal structures, electronic band structures, optical and electrical as well as transport properties of nanostructured Cu_xO are discussed. This section also describes the effect of doping or the presence of impurities on the properties of nanostructured Cu_xO.

2.1 Crystal structure

CuO has a black colour and crystallizes in the monoclinic centered Bravais lattice in the space group of $C2/c$. The crystallographic properties of CuO are tabulated in Table 1.[2,15,16,18] The copper atom is coordinated to four coplanar oxygen atoms situated at the corners of a rectangular parallelogram, which forms chains by sharing edges. The oxygen atom is coordinated to four copper atoms situated at the corners of a distorted tetrahedron. The chains traverse the structure in the [110] and [$\bar{1}$10] directions. The two types of chains alternate in the [001] direction and each type is stacked in the [010] direction with a separation between the chains of about 2.7 Å.[16,18,19] Fig. 1a demonstrates the crystal structure of CuO.

Cu_2O is the second stable phase of copper-oxide compounds which is reddish in colour. Cu_2O has a cubic structure (space group, o_h^4 or $Pn\bar{3}m$) with a lattice constant of 4.2696 Å. Each Cu atom in the unit cell is coordinated by two oxygen atoms.[19] The crystallographic properties of CuO are tabulated in Table 1.[2,15,16,18] Fig. 1b demonstrates the crystal structure of Cu_2O.

Anthony Morfa earned his Ph.D in physical chemistry from the University of Colorado, Boulder in 2009 under the supervision of Dr Jao van de Lagemaat of the National Renewable Energy Laboratory. He then took a research fellow position at the University of Melbourne, with Prof. Paul Mulvaney before accepting his current Alexander von Humboldt Research Stipendium in the Fachbereich Physik at Freie Universität Berlin with Prof. Dr Michael Giersig. Throughout this time, his research focus has been on studying and enhancing the optical and electronic properties of advanced opto-electronic devices and materials.

Dr Anthony O'Mullane is an Australian Research Council Future Fellow and Senior Lecturer at the Queensland University of Technology (Australia). He received his Ph.D degree (2001) from University College Cork (Ireland) and completed postdoctoral fellowships at Technische Universitat Darmstadt (Germany), the University of Warwick (UK), and Monash University (Australia). He previously held a position (2008) at RMIT University (Australia) until moving to QUT in 2013. Dr O'Mullane's research interests are the electrochemical synthesis and characterisation of nanostructured materials; electrocatalysis; catalysis; semi-conducting charge transfer complexes; Li batteries; and the application of electrochemical methods to various aspects of physical, chemical and biological science.

Kourosh Kalantar-zadeh is a Professor at RMIT University, Australia. He received his B.Sc. (1993) and M.Sc. (1997) degrees at the Sharif University of Technology, Iran, and Tehran University, Iran, respectively, and Ph.D at RMIT University, Australia (2002). His research interests include chemical and biochemical sensors, nanotechnology, microsystems, materials science, electronic circuits, and microfluidics. Prof Kalantar-zadeh is the Director of Centre for Advanced Electronics and Sensors (CADES) at RMIT University and the author of approximately 300 peer reviewed scientific papers and books. Prof Kalantar-zadeh is internationally recognized for his research on nanotechnology enabled sensors and two dimensional semiconductors.

5248 | *J. Mater. Chem. C*, 2014, **2**, 5247–5270

This journal is © The Royal Society of Chemistry 2014

Table 1 Crystallographic properties of CuO, Cu$_2$O and Cu$_4$O$_3$ (ref. 1–6)

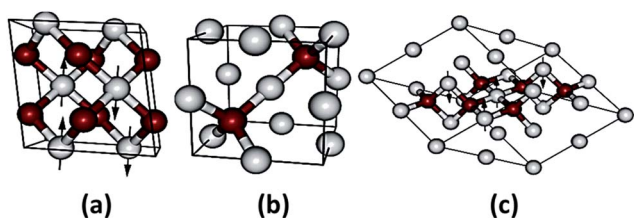|	CuO	Cu$_2$O	Cu$_4$O$_3$
Lattice	Monoclinic	Cubic	Tetragonal
	$a = 4.6837$ Å	$a = 4.2696$ Å	$A = 5.837$ Å
	$b = 3.4226$ Å		$b = 9.932$ Å
	$c = 5.1288$ Å		
	$\beta = 99.54°$		
	$\alpha = \gamma = 90°$		
Shortest distance			
Interatomic distances Cu–O	1.95 Å	1.84 Å	1.87 Å
Interatomic distances O–O	2.62 Å	3.68 Å	2.56 Å
Interatomic distances Cu–Cu	2.90 Å	3.01 Å	2.92 Å
Formula weight	79.57	143.14	302.18
Density	6.52 g cm^{-3}	5.75 g cm^{-3}	5.93 g cm^{-3}
Melting point	1201 °C	1235 °C	400 °C
Cell volume	81.08 Å^3	77.833 × 10^{-24} cm^{-3}	338 Å^3

Fig. 1 Monoclinic, cubic and tetragonal crystal structure of the copper oxide compounds (a) CuO, (b) Cu$_2$O and (c) Cu$_4$O$_3$ (gray and red spheres represent copper and oxygen atoms, respectively). For the antiferromagnetic CuO and Cu$_4$O$_3$ the arrows on the copper ions indicate the orientation of local magnetic moments. Reprinted figure with permission from (M. Heinemann, B. Eifert and C. Heiliger, *Phys. Rev. B*, 2013, **87**) copyright (2013) by the American Physical Society.

The third stable phase of copper-oxide with an atomic ratio of 1.33 is Cu$_4$O$_3$.[20] Cu$_4$O$_3$ is a mixture of Cu(I)/Cu(II) oxide. The local coordination environments of Cu(I) and Cu(II) are similar to the ones found in Cu$_2$O and CuO.[21] This less studied compound of the Cu$_x$O family was first discovered in 1870 as a mineral in the Copper Queen mine (Arizona, US).[2] Cu$_4$O$_3$ belongs to the tetragonal structure (space group, $I4_1/amd$) with a lattice constant of $a = 5.837$ Å and $c = 9.932$ Å.[21] Fig. 1c demonstrates the crystal structure of Cu$_4$O$_3$. From the crystal structure, one can observe that there are two types of copper ions which are Cu$^+$ and Cu^{2+}. The Cu$^+$ ion has two oxygen atoms as nearest neighbours forming collinear bonds of length 1.87 Å which is similar to cuprite (Cu$_2$O $\sim$ 1.85 Å). Similarly, the Cu^{2+} ion is surrounded by four oxygen atoms with bond lengths and angles being very close to those observed in tenorite (CuO).[18,19,21] The crystallographic properties of Cu$_4$O$_3$ are tabulated in Table 1.[2,21,22]

2.2 Electronic band structure

The reported band gap (E_g) values for CuO, which is a p-type semiconductor, are generally in the range of 1.2 to 2.16 eV.[1,23–27]

This wide range is attributed to several factors, including interpretation of the nature of the gap (*i.e.* direct or indirect), annealing treatment, grain dimensions, morphology and doping.[1,25,28–30] According to the Tauc relationship, for photon energies (E) greater than the band gap energy, the light absorption can be approximated using:[31]

$$\alpha E = \alpha_o (E - E_g)^\eta \tag{1}$$

where α is the absorption coefficient, α_o is a constant, E_g is the band gap energy and η is an exponent that depends on the type of transition involved. The value of η is $\frac{1}{2}$ or 2 for direct or indirect transitions, respectively. Rakhshani *et al.* have reported detailed studies of band gap determination of RF sputtered CuO films.[23] They found that their CuO films exhibited an indirect transition with a band gap of 1.21 eV. In contrast, Pierson *et al.*, while reporting the same deposition technique (RF sputtering), determined that their CuO films exhibited a direct band gap with a value of 1.71 eV.[32] The different values of E_g were due to different models $((\alpha E)^2$ or $(\alpha E)^{\frac{1}{2}})$ being used to determine the band gap value. The other significant factor that contributes to the variation of band gap values of CuO films is related to the heat treatment.[29,30] Izaki *et al.* demonstrated that annealing electrodeposited CuO films altered the E_g value.[29] They reported a reduction of 7.5% in E_g after annealing the as-deposited CuO at 773 K. They suggested that the changes in the composition, grain size and lattice constant were induced by the annealing process, altering the CuO band gap.[29]

In nanostructured CuO, the band gap generally increases with reducing crystallite dimensions.[1,33] Experimentally, this is often observed as a blue shift of the optical absorption band-edge when the nanostructure dimensions are reduced. The blue shift can be attributed to the quantum confinement (QC) effect.[1,34,35] The strong QC effect occurs when the size of the crystal is reduced much smaller than the Bohr radius for the material (≈ 6.6 nm for CuO).[1] This causes direct changes to the electron wavefunctions and hence significantly alters the E_g. A weak QC effect occurs when the crystal size is larger than the Bohr radius. This causes indirect perturbation of the electron wavefunction due to Coulomb effects and results in more subtle changes in the band gap energy.[34,35] In a recent study conducted by Rehman *et al.*, different scales of CuO nanoparticles were reported, where the crystallite dimension is controlled by annealing.[33] The crystallite dimensions obtained ranged from 11 nm ($T = 250$ °C) to 20 nm ($T = 600$ °C). They reported a reduction of 7% in direct E_g with an increase of crystallite dimensions.[33] In addition, it has been reported that the band gap values of nanostructured CuO can be tuned *via* engineering the morphology[36–38] as well as doping.[39–42]

Cu$_2$O is also a p-type semiconductor material due to the presence of copper vacancies.[2,43] It is a direct band gap material with $E_g > 2.1$ eV. However the band gap can be tuned *via* engineering the grain dimensions.[24,28,30,44,45] This observation is widely attributed to the QC effect in smaller grains, causing a blue shift in the band gap.[34,35,46] In a recent study conducted by Poulopoulos *et al.*,[46] on Cu$_2$O thin films with thicknesses

This journal is © The Royal Society of Chemistry 2014

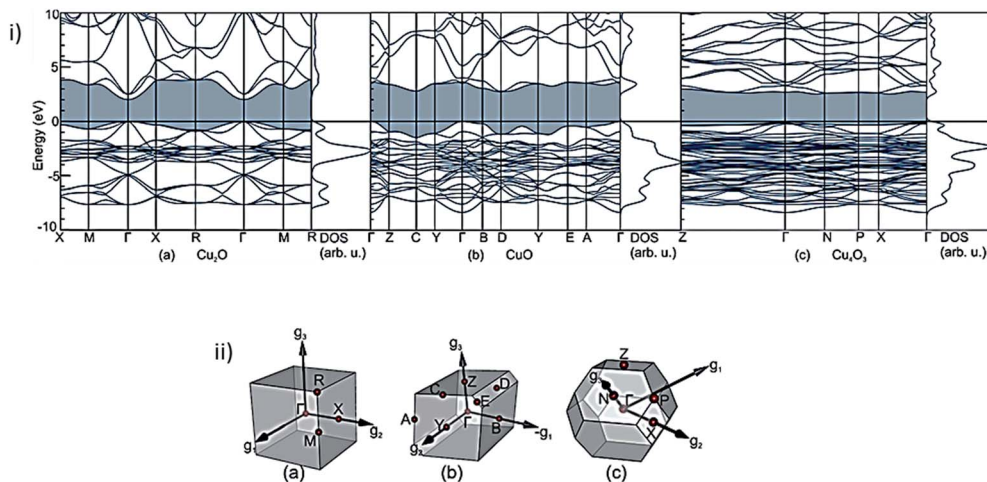*J. Mater. Chem. C*, 2014, **2**, 5247–5270 | 5249

Fig. 2 (i) Electronic band structure and density of states from hybrid functional DFT calculations and (ii) Brillouin zones with special high symmetry *k* points of the three copper oxide compounds to: (a) Cu$_2$O, (b) CuO and (c) Cu$_4$O$_3$. Reprinted figure with permission from (M. Heinemann, B. Eifert and C. Heiliger, *Phys. Rev. B*, 2013, **87**) copyright (2013) by the American Physical Society.

ranging from 0.75 to 5.4 nm the E_g value increased significantly from ~2.6 eV (5.4 nm film thickness) to ~3.8 eV (0.75 nm film thickness) due to QC effects. In addition, Balamurugan *et al.*[45] and Chang Y *et al.*[44] also reported on the observation of QC effects in Cu$_2$O. They further studied the effect of temperature[45] and annealing duration[44] on manipulating the crystallite sizes and hence altering the band gap of Cu$_2$O.

Similar to CuO, the optical band gap of Cu$_4$O$_3$ has also been reported with a wide range of values from 1.34 to 2.47 eV which can also be attributed to the interpretation of the type of band gap and whether direct or indirect transitions are allowed.[20,32,47,48]

A good comparison between the electronic properties of the three types of Cu$_x$O is presented *via* the band structure density functional theory (DFT) calculations by Heinemann *et al.* (Fig. 2i).[19] Fig. 2ii illustrates the Brillouin zones with special high symmetry *k* points of the three copper oxide compounds, which were used for the band structure DFT calculations.[19]

2.3 Optical properties

The optical behaviour of Cu$_x$O films have been experimentally studied, in particular the complex dielectric function ($\varepsilon(E) = \varepsilon_1(E) + i\varepsilon_2(E)$) was determined *via* spectroscopic ellipsometry.[2,49,50] For comparison, the imaginary part (ε_2) of the dielectric function for CuO, Cu$_2$O and Cu$_4$O$_3$ is shown in Fig. 3(a) and (b) with Gaussian fitting marked with numbers 1 to 7. For Cu$_2$O the peaks originate from the various band gaps corresponding to 2.59 eV (1), 2.71 eV (2),… 5.24 eV (7).[2] The difference in energy between these two first peaks is attributed to the spin–orbit splitting energy of ~0.12 eV for Cu$_2$O.[49] The absence of any sharp peaks for the CuO (ε_2) spectrum is due to low symmetry of this crystal. Similarly no sharp peak is seen for Cu$_4$O$_3$ for energies of less than 3.7 eV.

There are many reports regarding the absorption coefficient α (*E*) and normal-incidence reflectivity $R(E)$ of Cu$_x$O films in optical ranges.[2,49–51] Cu$_2$O is expected to have an essentially full Cu 3d shell with a direct forbidden band gap of 2.17 eV in the

bulk, which can only absorb light up to the visible region. In contrast, CuO has an open 3d shell with a direct band gap (1.2 eV in bulk) of charge-transfer type, which can absorb light up to the near infrared (IR) region.[1,15,27] A detailed analysis of the absorption coefficient obtained on bulk and thin film Cu$_2$O can be found in the report by Malerba *et al.*[51] Additionally, Rehman *et al.* and Borgohain *et al.* reported the optical absorption properties of CuO and Cu$_2$O nanoparticles of different sizes, respectively.[33,52] A comparative study of optical absorption between nanoparticles and near-monodisperse nanospheres of Cu$_2$O has been reported by Zhang *et al.*[53] They found that the nanospheres of Cu$_2$O have a wide absorption peak at 520 nm while Cu$_2$O nanoparticles have an absorption edge at 550 nm.[53]

Mayer *et al.* have reported that CuO is nonluminescent.[2] This is despite a few reports demonstrating the photoluminescence (PL) of CuO films, however the purity of such films is questionable (the presence of Cu$_2$O is a possibility). Nevertheless, Zhang *et al.* reported a detailed analysis of the PL properties of CuO nanostructures. They found that the PL properties of nanostructured CuO can be controlled *via* altering their shape, dimension and morphology.[1] The QC effect and the specific surface effect are the two most reported mechanisms which can
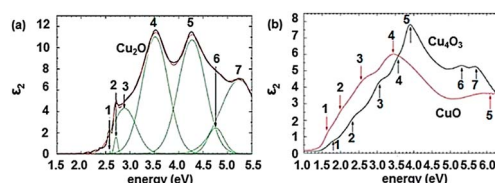

Fig. 3 Gaussian fit to the imaginary part of the dielectric ε_2 for (a) Cu$_2$O, (b) CuO and Cu$_4$O$_3$. Reprinted with permission from (B. K. Meyer, A. Polity, D. Reppin, M. Becker, P. Hering, P. J. Klar, T. Sander, C. Reindl, J. Benz, M. Eickhoff, C. Heiliger, M. Heinemann, J. Blaesing, A. Krost, S. Shokovets, C. Mueller and C. Ronning, *Phys. Status Solidi B*, 2012, **249**, 1487–1509) copyright (2012) by WILEY-VCH Verlag GmbH & Co. KGaA, Weinheim.
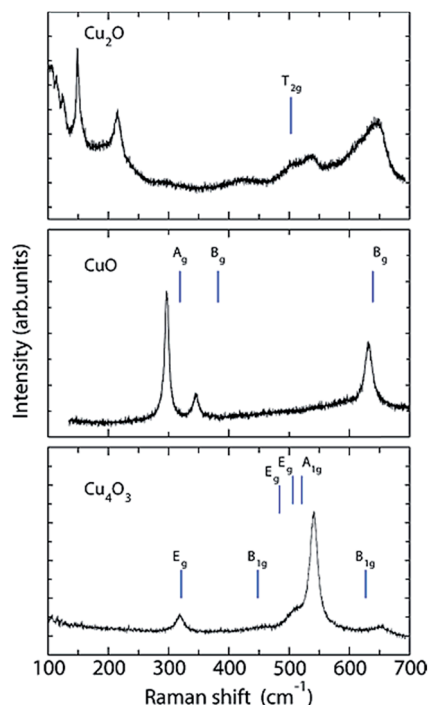
5250 | *J. Mater. Chem. C*, 2014, **2**, 5247–5270

This journal is © The Royal Society of Chemistry 2014

Fig. 4 Experimental Raman spectra of Cu_2O, CuO and Cu_4O_3. The calculated frequencies of Raman active vibrational modes are indicated by vertical bars. Reprinted with permission from (L. Debbichi, M. C. M. de Lucas, J. F. Pierson and P. Kruger, *J. Phys. Chem. C*, 2012, **116**, 10232–10237) copyright (2012) American Chemical Society.

result in the blue shift and red shift of the PL peak, respectively.[1,54] On the other hand, Cu_2O shows a weak PL effect due to the fact that optical transitions require parity change, which does not exist between the energetically highest valence band and lowest conduction band of the Cu_2O direct transition band.[2] In bulk Cu_2O, there are three peaks or shoulders that can be assigned to doubly charged oxygen vacancies (V_o^{2+}) at 1.72 eV (720 nm), singly charged oxygen vacancies (V_{cu}^{1+}) at 1.53 eV (810 nm) and copper vacancies (V_{cu}) at 1.35 eV (920 nm).[2] In nanostructured Cu_2O, these peaks and shoulders can be tuned *via* shape, dimension and morphology alterations as observed by Shi *et al.*[55,56]

2.4 Vibrational properties

The lattice dynamics of Cu_xO materials have been studied using IR, Raman and photoluminescence spectroscopy.[57–61] These studies provided insight into the nature of the electron phonon interaction and the negative thermal expansion (NTE) in Cu_xO. These methods also provided information about spin-phonon interaction and size dependent electron phonon scattering.[61] Debbichi *et al.* reported an extensive study of vibrational properties of Cu_xO *via* Raman spectroscopy where they clearly distinguished the different types of vibrational modes either by Raman or IR spectroscopy.[61] Recently, Shih *et al.* have reported studies on the size effects of spin-phonon coupling in in-plane CuO nanowires.[62] They employed low-temperature Raman spectroscopy for probing the local atomic vibrations of

nanowires. They found that the spin-phonon mode varies with the size of the CuO nanowires due to the increase in the strength of the spin-phonon coupling.[62]

The IR spectroscopy modes are associated with the relative motion of both copper and oxygen atoms which consist of asymmetric Cu–O stretching and asymmetric O–Cu–O bending modes. In contrast, Raman active modes only involve the relative motion of oxygen atoms.[63] Fig. 4 shows Raman spectra of Cu_xO with calculated frequencies of Raman active vibrational modes.[61] The symmetries of the zone-center modes are given by the following representations:[2,61]

$$\Gamma_{Cu_2O} = A_{2u} + E_u + 3T_{1u} + T_{2u} + T_{2g} \tag{2}$$

$$\Gamma_{CuO} = A_g + 2B_g + 4A_u + 5B_u \tag{3}$$

$$\Gamma_{Cu_4O_3} = 3E_g + A_{1g} + 2B_{1g} + 9E_u + 6A_{2u} + 5B_{2u} + 2B_{1u} + 2A_{1u} \tag{4}$$

2.5 Electrical properties

The electrical conductivity and hole density of p-type Cu_2O films vary with copper vacancy density, which act as shallow acceptors.[2] Similarly in CuO, copper deficiencies account for the intrinsic p-type semiconducting behaviour.[64] Suda *et al.* and Young *et al.* have studied the effect of temperature on electrical conductivity of CuO and Cu_2O films, respectively (Fig. 5(a) and (b)).[65,66] They have shown that an increase in temperature increases the conductivity of CuO and Cu_2O due to an increase in the hole concentration.[65] Similar findings were also reported by Gopalakrishna *et al.*[67] using Hall effect studies. They revealed a significant increase in conductivity, mobility and carrier concentration of nanocrystalline CuO after annealing.[67] Apart from temperature, electrical properties of Cu_xO also relied on grain dimensions, grain boundary, film thickness, specific phase and dopants.[1–3,68–72] Shao *et al.* reported an electrical conductivity of individual single CuO nanowires grown by thermal oxidation.[69] The electrical transport measurement has shown that the CuO nanowire has a conductivity of 7.8×10^{-4} $(\Omega \text{ cm})^{-1}$.[69] Additionally, Liao *et al.* reported that individual Cu_2O nanowires have a high mobility of $>95 \text{ cm}^2 \text{ V}^{-1} \text{ s}^{-1}$.[70] It is possible to tune the electrical properties (resistivity, carrier concentration and mobility) of Cu_xO by changing the stoichiometry and crystallinity of the Cu_xO films during the deposition process. Deposition parameters, such as pH of the solution in electrodeposition and hydrothermal methods and ion pressure and concentration in RF sputtering techniques, significantly contribute to changes in stoichiometry and crystallinity.[73–75]

2.6 Thermal properties

A limited number of studies have been carried out on the thermal properties of pristine copper oxide films. However, great interest has been shown for the development of nanoparticles of Cu_xO suspensions in fluids (nanofluids) due to the significant enhancement of thermal conductivity that they grant to the fluid in which they are suspended.[76–79] The relatively high thermal conductivity of CuO (76.5 W mK^{-1})[78] makes it an excellent candidate for enhancing the efficiency and reliability
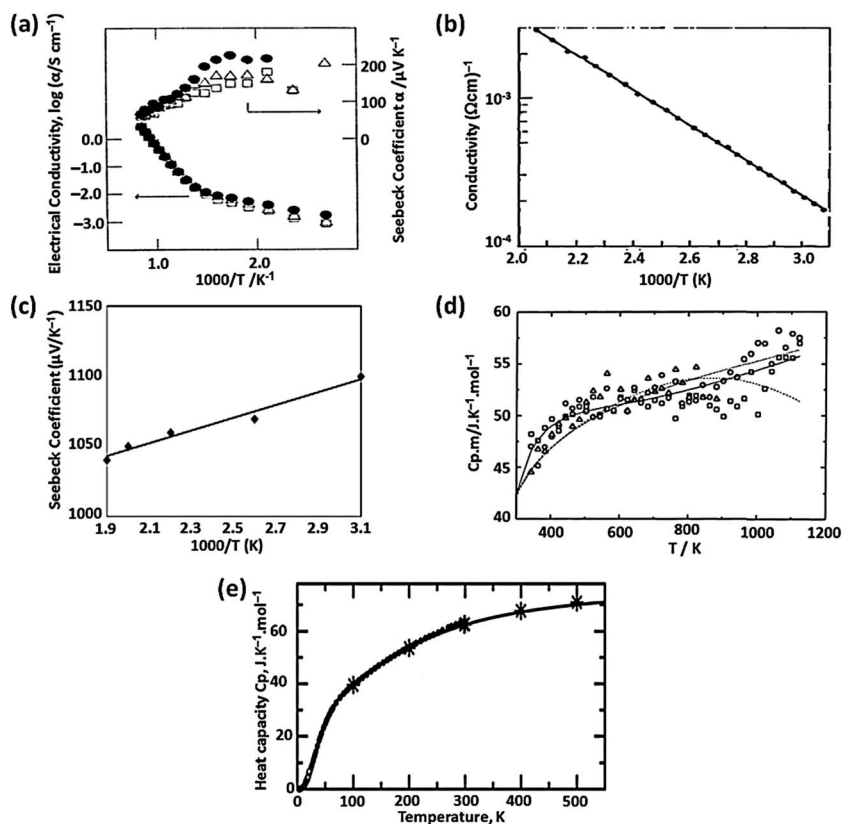
Fig. 5 (a) Temperature dependence for electrical conductivity and the Seebeck coefficient of CuO in oxygen (●), in air (Δ) and in 3% O_2–Ar (□), (b) electrical conductivity of Cu_2O single crystal vs. $1/T$, (c) Seebeck coefficient of Cu_2O single crystal vs. $1/T$, calculated and experimental heat capacities, C_p of (d) CuO: (□ Δ ○) ref. 89, (···) ref. 90, (- - -) ref. 91, and (e) Cu_2O: (—) ref. 88, (○) ref. 92 (●) ref. 93. Reprinted with permission from (a) (S. Suda, S. Fujitsu, K. Koumoto and H. Yanagida, *Jpn. J. Appl. Phys. 1*, 1992, **31**, 2488–2491) copyright (1992) by The Japan Society of Applied Physics, (b and c) reprinted from A. P. Young and C. M. Schwartz, *J. Phys. Chem. Solids*, 30, 249–252, copyright (1969) with permission from Elsevier, (d) reprinted from *Thermochim. Acta*, 348, J. Leitner, D. Sedmidubský, B. Doušová, A. Strejc and M. Nevřiva 49–51, copyright (2000) with permission from Elsevier, (e) (P. A. Korzhavyi, I. L. Soroka, E. I. Isaev, C. Lilja and B. Johansson, *P. Natl. Acad. Sci. USA*, 2012, **109**, 686–689) copyright (2012) National Academy of Science, USA.

of refrigeration and air conditioning systems.[80,81] In contrast, Cu_2O has a rather low thermal conductivity of the order of 4.5 W mK^{-1}.[82,83] It has been shown that the thermal conductivity enhancement of both CuO and Cu_2O nanofluids corresponds to an increased particle volume fraction and temperature.[84–87]

The variations in the Seebeck coefficient (S) of CuO and Cu_2O as a function of temperature are shown in Fig. 5(a) and (c) for which both oxides show decreasing trends. It has been shown that at 500 K, CuO and Cu_2O exhibit a maximum value of 200 μV K^{-1} and 1050 μV K^{-1}, respectively.[65,66]

The presence of a wide gap in the phonon spectra between low frequency (due to acoustic and optical phonon modes that involve the motion of Cu atoms) and high frequency (due to optical modes of oxygen vibrations) bands are reflected in the temperature dependence of heat capacity.[88] The calculated and experimental heat capacities (C_p) of CuO and Cu_2O as a function of temperature are shown in Fig. (5d) and (e).[88–93] As seen from the figure, the shape of C_p vs. temperature curves for both CuO (for temperatures below 800 K) and Cu_2O (for temperatures below 500 K) are accurately accounted for by the calculations that employ the quasi-harmonic approximation.[88]

2.7 Magnetic properties and superconductivity

The copper–oxygen covalent bond is the prominent factor governing the properties of high transition temperature (High-T_c) superconducting Cu_xO compounds.[94] Both CuO and Cu_4O_3 have an antiferromagnetic ground state. For CuO the antiferromagnetic unit cell has twice the size of the primitive unit cell of the crystal.[19] In the case of Cu_4O_3, it was suggested that the antiferromagnetic unit cell doubles the crystallographic unit cell in all three special directions.[19,95–97] Bulk CuO is antiferromagnetic with Néel temperatures from 213 K to 230 K.[1,98,99] The CuO antiferromagnetic transition takes place in two stages: near 230 K it leads to incommensurate antiferromagnetic order and near 213 K by a first order transition to a commensurate antiferromagnetic order.[94] As mentioned in Section 2.1, the copper atom of CuO is surrounded by four coplanar oxygen atoms, resulting in two sets of one dimensional Cu–O chains. The magnetic interaction due to super exchange leads to antiferromagnetic order in the Cu–O–Cu chains along the [10$\bar{1}$] direction with a bond angle of 146°.[94] Magnetic properties of nanostructured CuO significantly rely on their grain dimensions, morphology as well as anisotropy of the nanostructures.[1]

5252 | *J. Mater. Chem. C*, 2014, **2**, 5247–5270

This journal is © The Royal Society of Chemistry 2014

A diameter of 10 nm is the critical size for CuO nanoparticles to show ferromagnetic behaviour.[1,100–102] Interestingly, there are reports regarding room-temperature ferromagnetism of pure CuO nanostructures.[1,103–105] The room-temperature ferromagnetism is due to oxygen vacancies at the surface/or interface of the nanoparticles.[1,105]

A neutron diffraction study revealed that Cu_4O_3 undergoes a magnetic phase transition below 42.3 K leading to a pyrochlore lattice.[95,96] The amplitude of the magnetic moment carried by Cu^{2+} is $\sim$0.46 μ_β which indicates the strong covalent character of the Cu–O bonds and the presence of strong fluctuations even at low temperatures.[95]

Compounds made of Cu and O are the base of a famous class of high-T_c superconductors.[94] Superconductivity in these materials is observed when they are strongly doped away from their ideal stoichiometry. It has been shown that spatial changes in carrier density and the superconducting gap produce local inhomogeneity, which strongly affects their superconductivity.[106]

High-T_c was first discovered by Bednorz and Müller in 1986 using Cu and O compounds such as La_2CuO_4 doped with Ba.[107] A few months later it was found that doping the same material with Sr raised the superconducting critical temperature to nearly 40 K.[107] Recently, the performance of high-T_c copper and oxygen based materials was further enhanced with the inclusion of extra oxygen atoms as mobile "holes" into the copper oxide planes as illustrated in the $Bi_2Sr_2CaCu_2O_{8+x}$ and $YBa_2Cu_3O_{6+x}$ systems.[106,108] Apart from providing charge carriers, the role of oxygen dopants is still debatable and being investigated.[106,108–110]

2.8 Doping

It is possible to modify the chemical and physical properties of Cu_xO through doping. It has been shown that doping has the capability to alter the conduction type of Cu_2O (from p to n). Based on the valencies of Cu and O, which are +1 and −2 in Cu_2O, some n-type dopants including group VII elements such as halogens (O sites) (and possibly group II elements (Cu sites)) allow this transition to occur.[111] The typical reported halogen dopants include fluorine (F), chlorine (Cl) and bromine (Br) which can be intercalated into the structure of Cu_2O during the synthesis process.[111–114] Theoretically, F is the best match for O given the similarity in the size; however, CuF is soluble in water.[111] Recently, Scanlon et al. have demonstrated that intrinsic n-type defects or defect complexes in Cu_2O created during an electrodeposition process cannot be the source of any n-type behaviour.[75] They have suggested that the n-type conduction is due to an inversion layer which was attributed to a shallow donor level being formed during the electrodeposition process or due to external impurities (dopants).[75]

Generally, the hole density of native p-type Cu_xO films is poor, uncontrollable and sensitive to the preparation methods and experimental conditions. It has been reported that nitrogen (N) and silicon (Si) doped Cu_2O via a RF sputtering process can significantly reduce such instabilities.[115–118] These dopants were found to act as acceptors, which are incorporated into the oxygen lattice without converting the conduction type of Cu_2O.[117,118] To

further stabilize the films Ishizuka et al. and Okamoto et al. investigated the effect of passivation using hydrogen (H) and crown-ether cyanide of the N doped Cu_2O films.[115,119] The improvement after the treatment indicates that hole traps are passivated by cyanide or protons. These hole traps are generally due to oxygen vacancies or dangling bonds of Cu.[115]

For solar cell applications, the intrinsic photoconductivity of Cu_2O can be limited by minority charge carrier recombination caused by native defects acting as trap states. Isseroff et al. used first principles DFT calculations to study these trap states and demonstrated that substitutional cation doping reduces the recombination effect.[43] They found that split vacancies are the source of trap states that inhibit the minority carrier diffusion in Cu_2O. Dopants such as lithium (Li), magnesium (Mg), manganese (Mn), and zinc (Zn) prevent the formation of the split vacancies for a single cation vacancy which resulted in an electronic structure that exhibited no trap states within the band gap.[43]

3. Nanostructured Cu_xO synthesis

Many different approaches for the synthesis of nanostructured Cu_xO have been implemented using both vapour and liquid-phase-based methods. In this section, we present the most common synthesis methods and describe how they can be employed for engineering and tuning the morphologies and properties of Cu_xO.

3.1 Vapour phase synthesis

Vapour phase synthesis methods can be divided into two different categories: (i) physical vapour deposition (PVD) and (ii) chemical vapour deposition (CVD). The main difference between them is the process they employ, in which PVD uses physical forces to deposit films, while CVD uses chemical processes.

3.1.1 PVD methods. Many of the common PVD synthesis techniques such as RF sputtering, direct current (DC) sputtering, thermal evaporation, thermal oxidation, molecular beam epitaxy (MBE), pulse vapour deposition (PLD) and electron beam epitaxy (EBE) have been used for the deposition of nanostructured Cu_xO. A PVD process is purely physical, starting with either Cu_xO or Cu as the source material in the form of a solid target or powder, which is evaporated or sputtered with the application of ion bombardment, thermal heating, electron beam impingement or laser irradiation.

3.1.1.1 Sputtering. Amongst the PVD techniques, sputtering has, thus far, been the most common technique to synthesize thin film Cu_xO due to the ease of control over the deposition parameters. The as-synthesized films usually exhibit a nanometer-sized tightly packed columnar structure.[120–125] Sputtering is a process in which atoms are ejected from a solid target material by bombarding it with energetic particles. It offers a high degree of control over a film's crystallinity and stoichiometry. The crystallinity, grain dimension and stoichiometry of the copper oxide films can be controlled by varying the sputtering parameters such as applied power, oxygen flow rate,

oxygen partial pressure and concentration as well as annealing temperature.[32,120–122,124–128] For example, Chu *et al.* reported crystallite sizes of Cu_2O thin films varying from 16.8 to 8.8 nm when oxygen partial pressures increased from 1.1×10^{-3} to 1.8×10^{-3} Torr. This indicated that the higher the oxygen partial pressure, the smaller the crystallite size in the nanocrystalline Cu_2O thin films.[120] In contrast, Elfadill *et al.* reported that the crystallite size of CuO increased from 12 to 24 nm as the oxygen pressure increased.[125]

Generally in an oxygen rich sputtering chamber, at relatively low sputtering powers, only a small number of Cu atoms are sputtered, which effectively react with oxygen in the plasma, resulting in the deposition of films with high oxygen content such as CuO films. Conversely, Cu_2O films are formed at high sputtering powers, due to a large number of sputtered Cu atoms.[122,126] However, relatively high sputtering powers can also adversely affect the stoichiometry of the films, resulting in the presence of unreacted metallic copper and undesirable stoichiometric ratios between copper and oxygen.[122]

Although Cu_4O_3 was discovered during the late 1870s, the synthesis of single phase Cu_4O_3 thin films has rarely been reported. Pierson *et al.* and Richthofen *et al.* have successfully demonstrated the synthesis of single CuO, Cu_2O and Cu_4O_3 phases by varying the oxygen flow rate using a reactive magnetron sputtering technique.[32,128] They used a Cu target with the RF power maintained at 600 W. It was suggested that conductive Cu-rich copper oxide (Cu_4O_3) thin films tend to form at an oxygen flow rate $R(O_2) < 30\%$, whereas insulator O-rich copper oxide (CuO) thin films tend to form at $R(O_2) \geq 30\%$.[129] This is in contrast to the work of Blobaum *et al.* who also successfully synthesized Cu_4O_3 films *via* sputtering, but with a CuO target and at a lower sputtering power of 200 W.[127]

3.1.1.2 Thermal evaporation. Deposition of Cu_xO films using thermal evaporation is achieved by vaporizing a source material of Cu or Cu_xO (in either powder or condensed form) using heat either in a vacuum or in a controlled gaseous environment at a low pressure.[25,45,130–133] The vaporized Cu or Cu_xO that emanates from the material source interacts with the gas molecules in the environment of the deposition chamber before condensing onto a substrate. Processing parameters such as evaporation temperature, substrate temperature, substrate type, gas environment and pressure all play important roles in achieving the desirable Cu_xO thin films.[25,131,134] It has been reported that the as-synthesized Cu_xO films from these methods are usually compact thin films, which are textured by nanocrystallites (25–30 nm).[25,45,132,133]

3.1.1.3 Thermal oxidation. Thermal oxidation techniques offer a simple, convenient and fast method to synthesize nanostructured Cu_xO with various morphologies including nanowires, nanoribbons and nanorods.[135–139] In this method
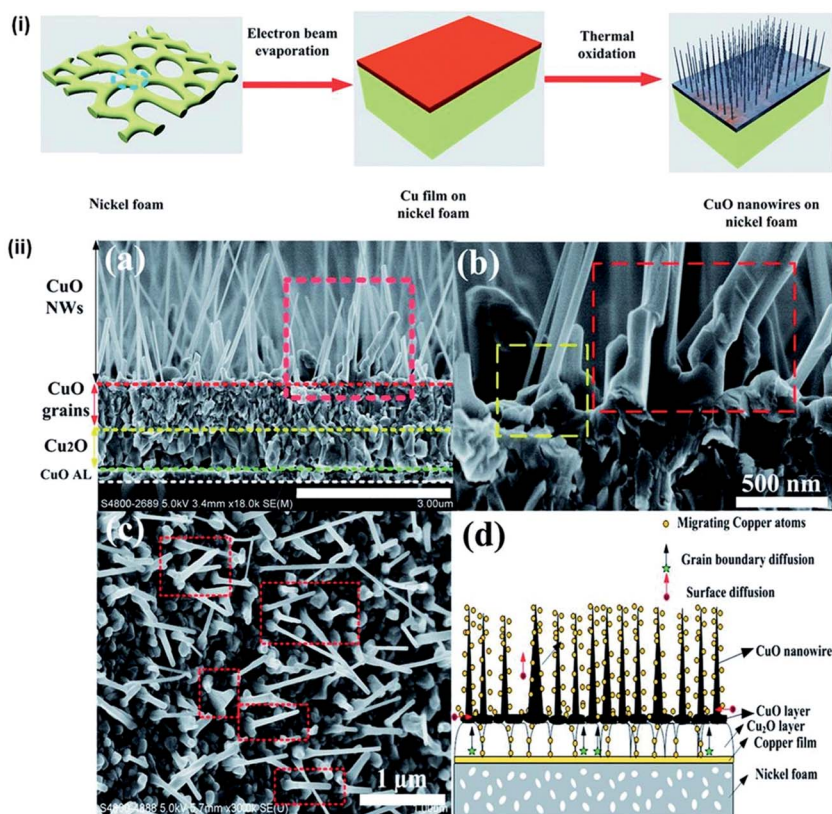
Fig. 6 (i) Schematic illustration of the synthesis process for CuO nanowires on nickel foam. (ii) (a) Cross-sectional view of CuO nanowires synthesized on the CuO adhesion layer (AL)/Si substrate, (b) magnified view from the nanowire root region marked by the red dashed square, (c) top-view of CuO nanowires synthesized on Ni foam and (d) illustration of the mechanism for CuO nanowire growth. Reproduced from ref. 148 with permission from The Royal Society of Chemistry.

5254 | *J. Mater. Chem. C*, 2014, **2**, 5247–5270

This journal is © The Royal Society of Chemistry 2014

nanostructured Cu_xO is directly grown on the surface of a Cu substrate.[137,138,140] Thermal oxidation is performed by simply heating a Cu substrate to a high temperature (typically between 200 and 800 °C) in an oxygen rich environment.[135,137,138,141–143] Generally, the morphology and stoichiometry of the Cu_xO can be controlled by tuning the deposition parameters. For instance, the diameter and density of Cu_xO nanowires can be altered by changing the oxidation temperature.[144] However, very high oxidation temperatures (>900 °C) are not suitable for nanowire formation as Cu_xO nanostructures can be fused together, as observed by Huang et al.[145] Valladares et al. have studied the effect of oxidation temperature in altering the stoichiometry of the Cu_xO films. They have observed that pure Cu_2O films are obtained at 200 °C, whereas CuO films are obtained above 300 °C.[143]

Unfortunately, mechanical adhesion between the as-deposited nanostructured Cu_xO and the substrates synthesized by the thermal oxidation method is very weak.[143,146–149] Cracking and flaking of the Cu_xO films or even exfoliation from the substrates poses a big challenge which severely affects the properties and practical applications of the nanostructured Cu_xO. Several methods have been proposed to alleviate the cracking and flaking problem including pre-deposition of a ZnO layer on copper foil,[150] synthesis of CuO nanowires on other foreign substrates such as silicon[147,151] or glass[152] and synthesis of CuO nanowires on porous substrates such as the porous copper substrate[149] or nickel foam[148] as shown in Fig. 6. Zhang et al. have successfully demonstrated non-cracked and flaked CuO nanowires synthesized on porous copper substrates. The porous substrates managed to reduce thermal stress during the oxidation process and as a result eliminate cracking and flaking issues.[149]

3.1.1.4 Other PVD methods. Apart from the aforementioned vapour phase methods, PLD[153–157] and EBE[158–161] deposition techniques are the other alternatives available for synthesizing Cu_xO films. It has been reported that the as-synthesized Cu_xO from these methods are usually compact thin films, which are textured by nanocrystallites (10–800 nm). The dimensions of the crystallites are significantly affected by the oxygen pressure and substrate temperature which were identified as being the two most important parameters.[154,155]

3.2 CVD methods

CVD processes have become the popular deposition techniques owing to their inherent flexibility and potential to tailor the Cu_xO phase composition by simply varying the operating conditions and precursors. Many forms of CVD have been used for depositing different Cu_xO stoichiometries, including atmospheric pressure CVD,[13,162,163] aerosol assisted CVD,[164–167] and plasma assisted CVD.[168] Such films are typically of a compact structure, consisting of micro- or nanometer-sized grains.

Generally, precursors such as bis-(2,4-pentanedionato) copper(II) or $Cu(acac)_2$ (acac = acetylacetonate) are used due to their high sublimation rate (activation energy of 105.6 kJ mol^{-1}) and low sublimation temperature between 140 and 190 °C.[162] Valtierra et al. have demonstrated the synthesis of nanostructured

Cu_4O_3 and CuO thin films with a crystallite size of 6.5 to 8.4 nm on fiberglass substrates using $Cu(acac)_2$ as a precursor and oxygen as a carrier-reactant gas via atmospheric pressure CVD.[162] The deposition temperature of CuO and Cu_4O_3 was recorded as 315 °C and 345 °C, respectively. In addition, thin films of Cu_2O have also been synthesized on fiberglass substrates using a similar technique and precursors by Ortiz et al. at a deposition temperature of 320 °C.[163]

However, precursors such as $Cu(acac)_2$, $Cu(dpm)_2$ (dpm = dipivaloylmethanate) and $Cu(hfa)_2$ (hfa = hexafluoroacetylacetonate) may present drawbacks in terms of poor thermal characteristics, reduced shelf life, halide incorporation or instability upon prolonged utilization due to aging phenomena.[169] Therefore, a second generation of adducts of the type $M(hfa)_2 \cdot$ tetramethylethylenediamine(TMEDA) (M = Cu(I) or Cu(II)) have been successfully adopted as alternative precursors.[169] They have favourable properties in terms of improved long-term stability and volatility with respect to conventional β-diketonate.[13,169] Barreca et al. were the first group to successfully demonstrate the deposition of nanostructured CuO and Cu_2O using the $Cu(hfa)_2$ adduct with TMEDA via CVD.[169] They successfully demonstrated morphological evolution from continuous films to 1D hyperbranched nanostructures.[169]

Spray pyrolysis is a typical aerosol-assisted chemical vapour deposition, which is utilized in the glass industry and in solar cell production to deliver film coatings of various thicknesses.[34] This method has the benefit of forming large-scale thin films by using a simple apparatus that can lead to increased productivity. Moreover, the film thickness and stoichiometry are easy to control and the resulting films are generally dense.[165,166] During film deposition, the precursor's solution is pumped to an atomizer, and then sprayed onto heated substrates. Subsequently the droplets undergo evaporation, solute condensation and thermal decomposition, which results in film formation.[34] The composition of these thin films is highly dependent on the solvent, morphology of the substrate as well as the deposition temperatures.[164,170]

Cu_xO films generated by the spray pyrolysis method are generally produced from copper acetate or copper nitrate as precursors dissolved in alcohol based solutions such as ethanol, propanol or methanol.[164,166,170,171] Alcohols are used to increase the wettability of the sprayed solution on the substrate and to improve the homogeneity of the deposited films.[165] It has been reported that Cu_xO nanostructures are formed with the addition of glucose or sucrose to the solution.[165,167] These sugars are used as reducing agents in the precipitation of the Cu_xO nanostructures.[165] Waser et al. demonstrated synthesis of CuO nanoparticles via flame spray pyrolysis with various diameters from 6 to 50 nm by varying the precursor solution and the oxygen flow rate.[172]

Apart from CuO and Cu_2O films, Cu_4O_3 films can also be obtained via spray pyrolysis techniques. Albores et al. have successfully demonstrated the deposition of Cu_4O_3 films on ZnO nanorods.[170] The formation of Cu_4O_3 films is a gradual process. Initially, the possible lattice matching of ZnO and CuO promotes the growth of CuO. In the presence of methanol, at elevated temperatures, the Cu^{2+} in CuO is reduced to Cu^{1+} forming Cu_2O as:[170]
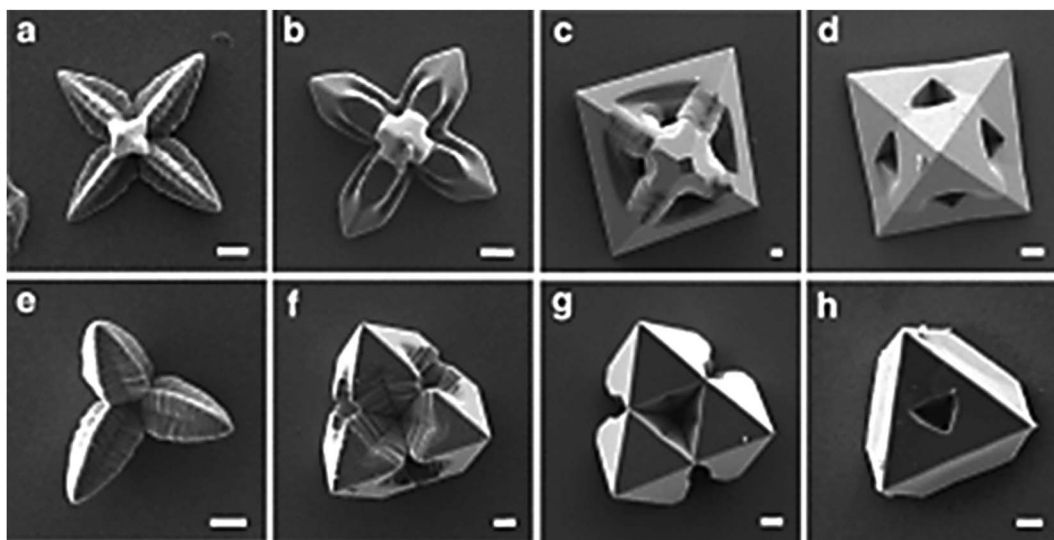
Fig. 7 SEM images of deposited octahedral Cu_2O crystals that display systematically varying degrees of branching with (100) planes parallel to the substrate (a–d) and with (111) planes parallel to the substrate (e–h). These crystals were obtained at a constant temperature (60 °C) and concentration of Cu^{2+} (0.02 M) and by applying deposition conditions of 0.10 mA cm^{-2} ≤ I ≤ 0.12 mA cm^{-2} and 0.08 V ≤ E ≤ 0.12 V. All figures have scale bars of 1 μm. Reprinted with permission from (M. J. Siegfried and K. S. Choi, *Angew. Chem. Int. Ed.*, 2005, **44**, 3218–3223) copyright (2012) by WILEY-VCH Verlag GmbH & Co. KGaA, Weinheim.

$$CH_3OH_{(g)} + 6CuO \rightarrow 3Cu_2O + CO_{2(g)} + 2H_2O_{(g)} \quad (5)$$
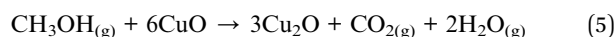
Then at these elevated temperatures, the solid reaction between CuO and Cu_2O results in paramelaconite phase formation which can be described by:[170]

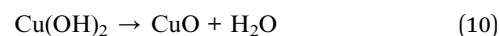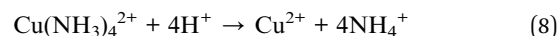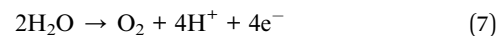$$2CuO + Cu_2O \rightarrow Cu_4O_3 \quad (6)$$
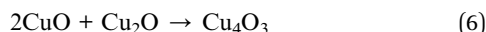
3.3 Liquid phase synthesis

Liquid phase techniques include methods such as electrode-position, hydrothermal/solvothermal and sol–gel. These methods are generally chosen due to their low capital cost and better control of the material's morphology in comparison to vapour phase deposition techniques as well as the deposition at relatively low temperatures, which is crucial for low-heat-tolerant substrates. Among a variety of liquid phase synthesis methods, hydrothermal/solvothermal and chemical precipitation techniques have been widely used to synthesize Cu_xO nanostructures.

3.3.1 Electrodeposition. Electrodeposition is a process in which metal ions in an electrolyte are reduced at a conducting electrode under potential control. The process uses electrical current to reduce Cu^{2+} ions from an aqueous solution. The electrolyte generally contains a mixture of a Cu salt such as copper sulphate, copper acetate or copper nitrate and a chelating agent such as lactic acid, ammonium nitrate, amino acids or tartaric acids.[29,173–177] The deposition is carried out in an alkaline environment with the addition of sodium hydroxide or ammonia to control the pH level. The electrodeposition technique is commonly used for depositing CuO and Cu_2O films.[3,29,173–175,177–180] Such films are typically of a compact structure, consisting of micro- or nanometer-sized grains. The stoichiometry of the electrodeposited films is very much dependent on the type of the chelating agent and applied potential used during the electrodeposition process. Generally, CuO films are obtained upon the application of a positive voltage/current bias, where oxidation of Cu is expected and this process is well known as anodic electrodeposition. Inversely, Cu_2O films are deposited at a negative bias, in which the reduction process occurs (cathodic electrodeposition).[173,174,181]

Synthesis of CuO films *via* anodic electrodeposition in an alkaline solution containing copper(II) nitrate, ammonium nitrate and ammonia has been reported by Izaki *et al.* at +0.9 V *vs.* Ag/AgCl.[174] Sasano *et al.* demonstrated that CuO films formed by applying potential pulses are more crystalline than the ones deposited using a constant potential.[176] The mechanism for the electrodeposition of CuO films is outlined in eqn (7)–(10). The reaction starts *via* electrolysis of water to generate oxygen and protons (reaction (7)). Consequently, these protons react with ammonia Cu(II) complexes to yield free Cu(II) ions in the vicinity of a substrate's surface (reaction (8)). The free Cu(II) ions are then hydrolyzed to form CuO films on the substrate (reactions (9) and (10)).[174,181]

$$2H_2O \rightarrow O_2 + 4H^+ + 4e^- \quad (7)$$

$$Cu(NH_3)_4^{2+} + 4H^+ \rightarrow Cu^{2+} + 4NH_4^+ \quad (8)$$

$$Cu^{2+} + 2OH^- \rightarrow Cu(OH)_2 \quad (9)$$

$$Cu(OH)_2 \rightarrow CuO + H_2O \quad (10)$$

Similarly, syntheses of Cu_2O films have been reported *via* cathodic electrodeposition using an alkaline aqueous solution containing copper(II) sulphate or copper(II) acetate and lactic acid as the chelating agent.[10,173,175,179,180,182] Zoolfakar *et al.* have

5256 | *J. Mater. Chem. C*, 2014, **2**, 5247–5270

This journal is © The Royal Society of Chemistry 2014

demonstrated the electrodeposition of Cu_2O films onto ZnO for forming heterojunction solar cells.[173] The electrodeposition process was carried out at -0.55 V $vs.$ Ag/AgCl. Cu_2O was formed according to the following electrochemical reaction.[175]

$$2Cu^{2+} + 2e^- + 2OH^- \rightarrow Cu_2O + H_2O \qquad (11)$$
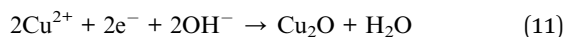
Apart from depositing thin films of Cu_xO, electrodeposition techniques have been used to synthesize various morphologies of nanostructured CuO and Cu_2O including leaf-like,[183] nanospindles,[184] nanocubes,[185] nanorod[186] and cauliflower-like.[187] Interestingly, Siegfried and Choi have demonstrated a new level of tuning and engineering the morphology of Cu_2O crystals via the electrodeposition technique.[188,189] They manipulated deposition parameters such as potential and current to engineer Cu_2O crystals as illustrated in Fig. 7.[189]

3.3.2 Hydrothermal and solvothermal. Hydrothermal and solvothermal processes are facile and cost-effective deposition techniques. They have the capability of producing nanostructured Cu_xO of different morphologies including nanodendrites,[190] nanowires,[71] nanorings,[191] nanorods,[192–195] nanoribbons,[191,194] nanotubes,[192] microspheres[194,196] and macrowhiskers.[197] (Fig. 8).

The synthesis of nanostructured Cu_xO has been hydrothermally achieved using various precursors such as copper(II) chloride, copper(II) acetate or copper(II) sulphate. Generally, a lower concentration of $Cu(OH)_4^{2-}$ precursors favours tubular formation, whereas a higher concentration leads to rodlike morphologies.[192,194] In most cases, the hydrothermal synthesis of Cu_xO starts with the preparation of a solution that contains copper salts, sodium hydroxide and solvents, typically deionized water. Such a solution is then kept at an elevated temperature (100–300 °C) for a certain period of time, allowing the nucleation and growth of Cu_xO crystallites.

Solvothermal methods are almost identical to hydrothermal methods except that organic solvents are used instead of water.[198,199] In comparison with the hydrothermal method, the solvothermal method exhibits many advantages such as easier morphological control, free foreign anions and macroscopic quantity.[200,201] Recent reports have shown that the high-aspect-ratio of Cu_xO nanostructures can be synthesized via solvothermal methods.[202–205] Zhao et $al.$ have demonstrated a facile method to synthesize pure polycrystalline Cu_4O_3 microspheres using copper(II) nitrate as the precursor in the presence of N,N-dimethylformamide and ethanol.[201] They have successfully manipulated the CuO/Cu_2O stoichiometry ratio to generate Cu_4O_3 films with the reaction of ($2CuO + Cu_2O \rightarrow Cu_4O_3$) in a closed system.[201]

3.3.3 Solution-based chemical precipitation methods. In most cases, the chemical precipitation synthesis of CuO nanoparticles starts with the preparation of a solution that contains copper salts, sodium hydroxide and solvents, typically deionized water. In order to avoid agglomeration of the CuO nanoparticles, an external energy such as ultrasonic or high pressure needs to be applied during the synthesis process. Zhu et $al.$ prepared highly dispersed CuO nanoparticles of 6 nm with various morphologies including spherical, ellipsoidal and
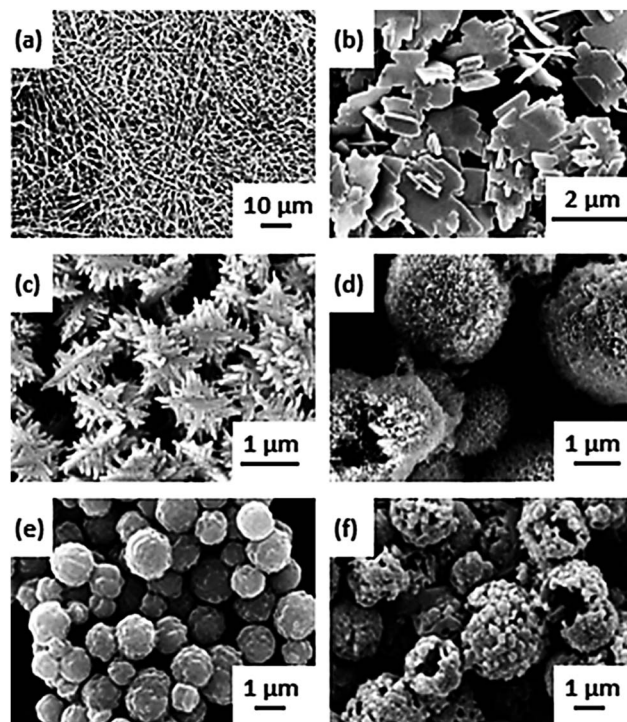

Fig. 8 SEM images of various morphologies via hydrothermally/solvothermally synthesized (a) Cu_2O nanowires synthesized at 180 °C in copper(II) acetate aqueous solution with pyrrole, (b) CuO flake-like synthesized at 200 °C in copper(II) sulphate aqueous, (c) CuO/Cu_2O dendrite-like synthesized at 200 °C in copper(II) sulphate aqueous with 10 ml ethylene glycol (EG), (d) CuO/Cu_2O flower-like synthesized at 200 °C in copper(II) sulphate aqueous with 20 ml EG, and CuO/Cu_2O composite hollow microspheres obtained in a copper(II) acetate aqueous solution at 200 °C for (e) 1 hour and (f) 5 hours. Reprinted with permission from (a) (Y. W. Tan, X. Y. Xue, Q. Peng, H. Zhao, T. H. Wang and Y. D. Li, $Nano$ $Lett.$, 2007, **7**, 3723–3728) copyright (2007) American Chemical Society, (b–d) (S. Z. Li, H. Zhang, Y. J. Ji and D. R. Yang, $Nanotechnology$, 2004, **15**, 1428–1432) copyright (2004) by IOP Publishing Ltd, (e and f) (H. Yu, J. Yu, S. Liu and S. Mann, $Chem.$ $Mater.$, 2007, **19**, 4327–4334) copyright (2007) American Chemical Society.

needle-shaped CuO.[206] Wu et $al.$ prepared CuO nanoparticles with different sizes and morphologies in organic solvents such as dimethylacetamide (DMAC).[207] They found that the nucleation and growth kinetics of CuO nanoparticles can be tuned by varying the processing parameters including the volume ratio of DMAC and water, increasing the temperature of the solution and the molar ratio of Cu^{2+} and OH^-.[207] Apart from nanoparticles, chemical precipitation synthesis has commonly been used to synthesize different morphologies of CuO including nanowires,[208–210] nanoribbons,[211] flower-like,[212,213] hierarchical nanochains[214] and nanosheets.[215,216] A recent comprehensive review on nanostructured CuO via the solution-based chemical precipitation technique is found elsewhere.[1]

There are many reports of synthesis of nanostructured Cu_2O via chemical precipitation.[53,217–224] Gou et $al.$ demonstrated a synthesis of highly uniform and monodisperse Cu_2O nanocubes. The process involved the use of sodium ascorbate to reduce Cu(II) salts in water, in the presence of a surfactant and NaOH. The nanocube dimensions were tuned by varying the

concentration of the surfactant.[217] Zhang *et al.* reported synthesis of monodisperse Cu_2O and CuO nanospheres. It has also been shown that by modulating the concentration of solvent, the diameter, crystallization and monodispersity of Cu_2O nanospheres can be kinetically controlled.[53] Interestingly, various groups have reported a facile method for the synthesis of Cu_2O nanocrystals with systematic shape evolution (Fig. 9).[220–223] Recently, Susman *et al.* demonstrated precise morphology control of Cu_2O nanocrystals covering the entire range of morphologies from complete cubes, *via* the intermediate morphologies truncated octahedral, cuboctahedra and truncated cubes, to complete octahedral.[220] The highly effective morphology control is attributed to competitive adsorption of hydroxide and citrate anions on the [100] and [111] planes of the growing crystallite.[220]

3.3.4 Other film formation methods. A sol–gel process involves the formation of a colloidal solution (sol) from selected chemicals that acts as a precursor for an integrated network
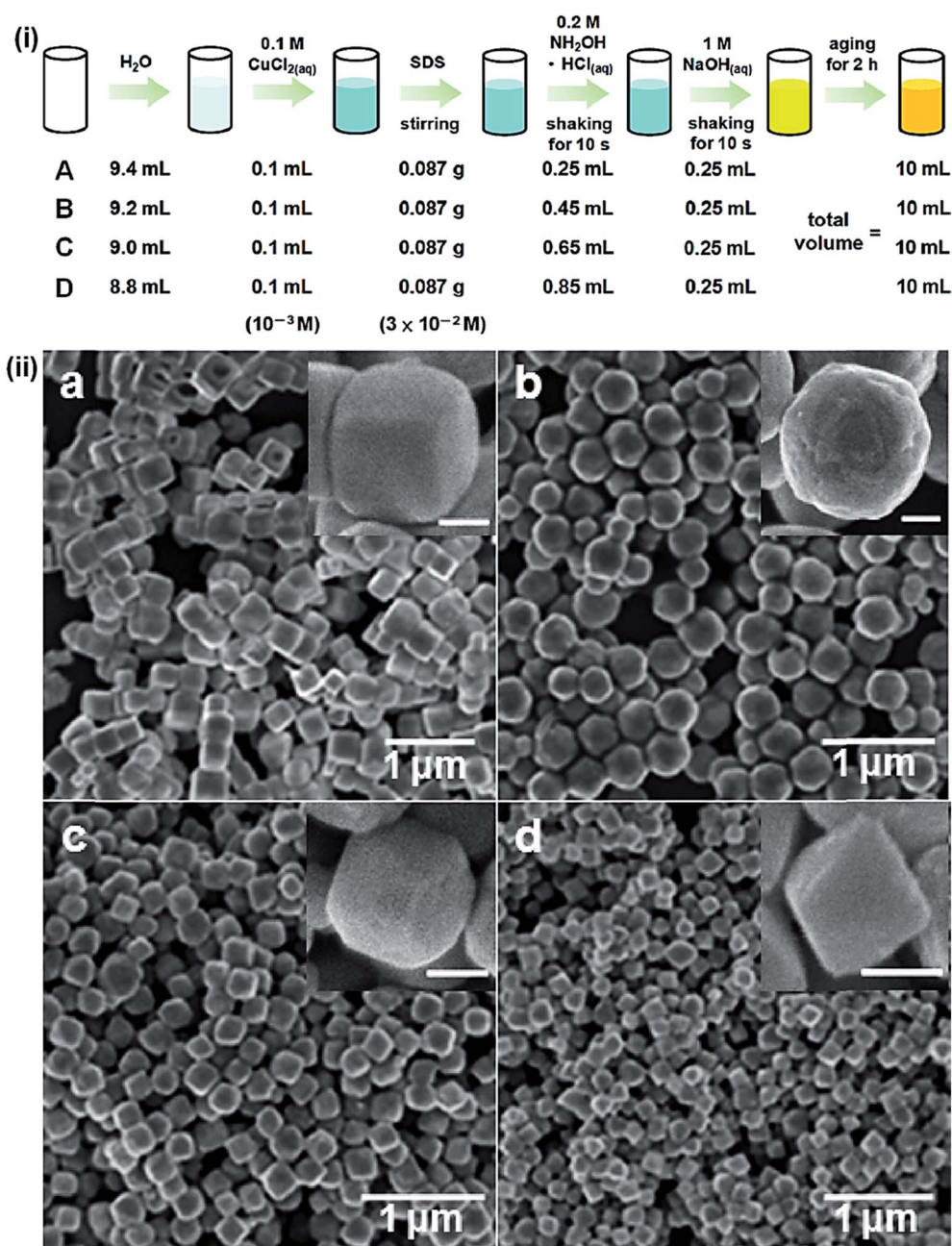
Fig. 9 (i) Schematic illustration of the procedure used for growing Cu_2O nanocrystals of different shapes. (ii) (a–d) Respective SEM images of the Cu_2O nanocrystals synthesized in sample containers A, B, C and D with increasing amounts of $NH_2OH\cdot HC$ added to the solutions. The particle morphologies are (a) truncated cubic, (b) cuboctahedral, (c) truncated octahedral and (d) octahedral in shape. Insets show the enlarged views of individual nanocrystals. The scale bars in the insets are 100 nm. Reprinted with permission from (C.-H. Kuo and M. H. Huang, *J. Phys. Chem. C*, 2008, **112**, 18355–18360) copyright (2007) American Chemical Society.

5258 | *J. Mater. Chem. C*, 2014, **2**, 5247–5270

This journal is © The Royal Society of Chemistry 2014

(gel) of either discrete particles or connected networks. During gelation (aging process), various forms of hydrolysis and poly-condensation processes can take place. Film deposition is generally carried out during the gelation process *via* dip-coating, spin coating or drop-casting onto the substrates. Armelao *et al.* have reported Cu_xO thin films *via* sol–gel synthesis, using ethanolic solutions of copper(II) acetate.[225] Films were obtained by dip-coating at room temperature in air and were subsequently heat-treated at different temperatures (100–900 °C) in oxidizing (air), inert (N_2) or reducing (4% H_2 in N_2) atmospheres to observe different crystalline phases of Cu_xO as a function of the annealing conditions with an average crystallite size lower than 20 nm.[225] Ray has also reported a similar technique, however he experimented with methanolic solutions of cupric chloride.[226] Under atmospheric heat-treatment conditions, Armelao *et al.* have only managed to observe the CuO phase with 900 °C annealing, while Ray has successfully demonstrated the deposition of CuO and Cu_2O at 360 °C and 400–500 °C, respectively.[225,226]

Templating is a modification of the sol–gel synthesis technique and can be very effective for the preparation of Cu_xO nanowires.[141] Nanostructured Cu_xO is deposited onto porous templates such as anodic alumina membranes and poly-carbonate membranes.[227–229] Generally, templates are used for assisting the growth of the Cu_xO by controlling the diameters, lengths and densities of the nanowires.[227] At the end of the deposition process, the templates must be removed either by chemical reactions[229] or a selective burn-away at high temperatures.[230] Consequently, this procedure may prolong the process as well as degrade the quality of the Cu_xO.[141]

4. Applications of Cu_xO

Cu_xO has been employed for a variety of applications ranging from optical devices to high thermal conductivity systems. In this section, some of the most common applications of Cu_xO materials are presented. Particular emphasis is placed on the enhancements that can be achieved by exploiting the nano-structured forms of Cu_xO.

4.1 Solar cells and light emitting diodes

Cu_xO films are possible candidates for developing different types of optical devices, including solar cells based on dye-sensitized and heterojunction architectures as well as organic light emitting diodes.

The quest and need for a clean and economical energy source have increased interest in the development of solar applications. Amongst various metal oxide materials for solar energy applications, Cu_2O has attracted increasing interest due to its theoretical power conversion efficiency (PCE) of 18% and an absorption coefficient higher than single crystalline Si.[173,231]

As described previously Cu_xO is an intrinsically p-type material. However, self-compensation problems and dopant solubility have inhibited the synthesis of n-type Cu_xO to produce efficient homojunctions for photovoltaic applications.[3,72,232] Therefore, heterojunction architectures have been

employed with other n-type semiconductors such as ZnO,[10,173,175] CdO,[233] TiO_2,[234–236] Ga_2O_3 (ref. 237) and GaN.[2] Amongst the aforementioned n-type semiconductors, ZnO has been found to be the most stable and exhibit relatively low lattice mismatch of 7.6% between the (002) ZnO and (111) Cu_2O phases.[3,175,177] Despite the predicted PCE value of 18%, in practice the ZnO–Cu_2O solar systems have yet to reach high efficiencies.[3,10,238] To date, the highest efficiency ever reported for bilayer ZnO–Cu_2O heterojunction solar cells has been 3.83%.[239] This is due to the fact that theoretically their intrinsic electronic band structures do not permit an open circuit voltage larger than 0.7 V.[238] To date, the largest ever short circuit current that has been reported by Zoolfakar *et al.* using electrodeposited ZnO and Cu_2O films was 12.7 mA cm^{-2} (Fig. 10).[173]

Apart from heterojunction cells, Cu_xO has also been widely used in dye-sensitized solar cell (DSSC) technology. CuO is commonly used as a blocking layer that prevents recombination reactions by forming a potential barrier between the anode and the electrolyte which enhances the PCE of the device.[240–243] Yet in other experiments, the use of Cu_2O at the photoanode of a DSSC was found to decrease the overall PCE.[244] This is due to the dissociation of Cu_xO in liquid-based electrolytes, inducing numerous extrinsic defects that increase carrier recombination, resulting in photovoltaic performance degradation.[244]

Cu_xO has also been used in organic light emitting diodes (OLEDs).[134,245] In order to construct efficient OLEDs, it is important to optimize the carrier injection ability at the interface of the active layer and anode materials. The Cu_xO films are commonly used as hole injection layers (HILs) to lower the hole injection barrier.[134,246,247] Kim *et al.* have reported the advantage of using a mixed stoichiometry of CuO and Cu_2O for increasing the performance of OLEDs as illustrated in Fig. 11.[134] Mixed stoichiometry of Cu_xO contains high density of defects such as oxygen vacancies or unbonded oxygen atoms, which act as an

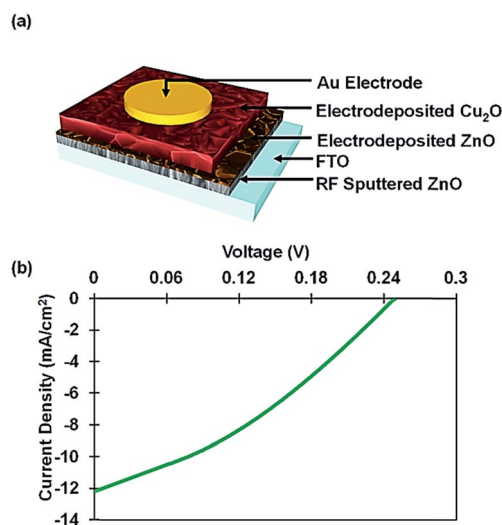**Fig. 10** (a) 3D schematic of the electrodeposited ZnO–Cu_2O heterojunction solar cells, (b) *J–V* characteristic curves of ZnO–Cu_2O heterojunction solar cells. Reproduced from ref. 173 with permission from The Royal Society of Chemistry.

This journal is © The Royal Society of Chemistry 2014

J. Mater. Chem. C, 2014, **2**, 5247–5270 | **5259**

extra energy state within the energy gap of the Cu_xO layer. Interestingly, when the energy levels of these gap states are aligned with the highest occupied molecular orbital (HOMO) level of the hole transporting layer, no potential barrier is produced at the anode interfaces, which can lead to an increase in the hole injection efficiency.[134]

4.2 Photo-catalytic applications

Cu_xO is a promising photo-catalyst that is used in many chemical processes, such as organic contamination degradation and water splitting under visible-light irradiation owing to

Fig. 11 (i) Phase diagram of a copper–oxygen binary system and the schematic diagram of electronic states and the film structure of stoichiometric and non-stoichiometric Cu_xO, (ii) (a) current–density voltage (J−V) and (b) luminance–voltage (L−V) characteristics of OLED with Cu_xO HIL deposited at different rates. Inset: schematic diagram of OLEDs. Reproduced from ref. 134 with permission from The Royal Society of Chemistry.

their small band gap and low cost.[13,248–255] Under illumination, Cu_xO produces electron/hole pairs that can generate hydroxyl radicals ($^{\bullet}HO$) from water. This radical is capable of mineralizing most organic molecules.[250] For water splitting applications, the majority charge carriers of the Cu_xO (holes) oxidize water to oxygen gas (O_2), while the photo-generated minority charge carriers (electrons) reduce water to hydrogen gas (H_2).[248,254,255] Significantly, the Cu_xO conduction band is more negative than the redox potential of H^+/H_2, which allows sunlight to produce H_2 from water.[253]

Unfortunately, the general photo-instability of Cu_xO greatly hinders its direct application in photo-catalysis.[248,256] To overcome this photo-instability effect, Cu_xO is typically coupled with other semiconductors to form heterojunctions and it has been reported that TiO_2 is one of the best candidates for this purpose.[256,257] Additionally, nanostructuring of Cu_xO can also significantly improve overall stability.[256] Fortunately, the large surface area to volume ratio, which is provided by nanostructuring, significantly increases the effective surface area available for photo-catalytic reactions.[249,250,252]

It has also been reported that the photo-catalytic production rate of H_2 can be significantly improved in the presence of alcohol, which provides suitable electron donors (also known as sacrificial agent/reagent).[258–260] Barreca et al. have successfully demonstrated excellent performance of Cu_2O photo-catalysis for generating H_2 in the presence of methanol.[13] They have suggested that methanol inhibits electron–hole recombination and acts partially as a hydrogen source.[13] However, efficient photo-catalytic activity of CuO for H_2 production has not been reported. This is despite the fact that the band gap of CuO is 1.2 eV, which makes CuO an efficient material to absorb sunlight. However, the position of the conduction band level limits its activity. Therefore, introducing a sacrificial agent is crucial to enable it to be used as a photo-catalyst. For example, Yao et al. have reported that CuO exhibits high photo-catalytic activity in oxalic acid solutions.[253] Oxalic acid, which is a common pollutant in industrial wastewater, is a strong reductive agent and acts as an electron donor.[261,262]

4.3 Antimicrobial applications

The antimicrobial properties of Cu_xO, in particular CuO, have attracted growing research interest. Nanostructured Cu_xO commonly offers a strong degree of chemical and physical stability. Most bacterial cells have cellular membranes that contain pores in the nanometer range. Cu_xO, with dimensions less than 20 nm, have shown antibacterial properties.[11,263] The antimicrobial activity of CuO has been attributed to the production of reactive oxygen species (ROS) such as $^{\bullet}O_2{}^-$, $^{\bullet}HO_2$, $^{\bullet}OH$ and H_2O_2 which can also occur without exposure to any visible light owing to the small band gap of CuO.[264,265] The generated ROS interact with outer cell walls to generate free radicals. The radicals penetrate into the inner cell membranes which lead to the disruption of the internal contents of the cell.[264,265] The effectiveness of the antimicrobial agent appears to be related to the nature of the cell wall structures.[263,265–267] S. aureus is composed of multiple layers of peptidoglycan with

5260 | J. Mater. Chem. C, 2014, **2**, 5247–5270

This journal is © The Royal Society of Chemistry 2014

numerous pores, which are suggested to be more susceptible to intracellular transductions. In contrast, the cell walls of *E. coli* are relatively thin, mainly consisting of peptidoglycan and outer layers of lipopolysaccharide, lipoprotein and phospholipids, which are less prone to being attacked by CuO nanoparticles. As a result, nanostructured CuO has a higher antimicrobial activity against *S. aureus* than *E. coli*.[263,264]

It has been demonstrated that nanostructured CuO antimicrobial activity can be enhanced by exposing it to light.[11,264,268–270] As described in Section 4.2, light irradiation generates excited electron–hole pairs in the CuO and deactivation of the bacteria is possible *via* a photo-catalytic process.[11,268] Akhavan *et al.* have reported an improvement of 22% of CuO antibacterial activity under illumination.[11]

Fig. 12 Cycling profile of (a) bare CuO, graphene and CuO/graphene electrode at a current density of 67 mA g^{-1}, (b) CuO nanoparticles with three types of morphologies (urchin-like, hollow cubes and hollow spheres) at a current density of 150 mA g^{-1}, (c) CuO hollow nanoparticles/graph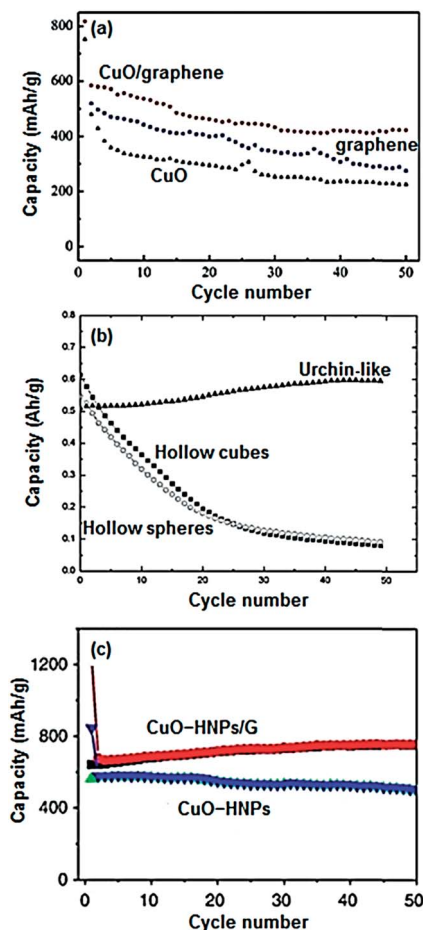ene (CuO−HNPs/G) and CuO hollow nanoparticles (CuO−HNPs) at 50 mA g^{-1}. (a) Reprinted from Y. J. Mai, X. L. Wang, J. Y. Xiang, Y. Q. Qiao, D. Zhang, C. D. Gu and J. P. Tu, *Electrochim. Acta*, **56**, 2306–2311, copyright (2011) with permission from Elsevier, (b) reprinted with permission from (J. C. Park, J. Kim, H. Kwon and H. Song, *Adv. Mater.*, 2009, **21**, 803) copyright (2009) by WILEY-VCH Verlag GmbH & Co. KGaA, Weinheim, (c) reprinted from J. Zhou, L. Ma, H. Song, B. Wu and X. Chen, *Electrochem. Commun.*, **13**, 1357–1360, copyright (2011) with permission from Elsevier.

4.4 Electrochemical applications

The electrochemical properties of nanostructured Cu$_x$O as electrodes for lithium ion batteries (LIB) have also been of growing research interest. Cu$_x$O has many attractive advantages over conventional materials including high theoretical capacity (>600 and >350 mA h g^{-1} for CuO and Cu$_2$O, respectively) and low cost.[271–273] One of the major issues with the use of Cu$_x$O in LIBs is its large volume variation during the Li$^+$ ion insertion/extraction processes, which leads to severe mechanical strains and a rapid decay in capacity.[271] Recently, there have been various reports demonstrating LIBs with high reversible capacity and cycling stability by synthesising Cu$_x$O/graphene nanocomposites.[271,274,275] Mai *et al.* reported an excellent reversible capacity of 583.5 mA h g^{-1} with high cycling stability by incorporating CuO nanoparticles (∼30 nm) onto graphene sheets (Fig. 12a). The graphene sheets serve as a conductive network for fast electron transfer as well as buffered spaces to accommodate the CuO volume expansion/contraction during the Li$^+$ insertion/extraction process.[274]

Nanostructuring Cu$_x$O into hollow nano/microstructures such as spheres, cubes or urchin-like structures increases its LIB performance.[201,275–277] For example, Park *et al.* have successfully demonstrated that hollow CuO urchin-like nanoparticles possess a charge capacity above 560 mA h g^{-1} (Fig. 12b).[276] Wei *et al.* have discussed and listed three main advantages of hollow structures as anode materials for LIBs.[277] Zhou *et al.* have reported excellent LIB performance by integrating hollow nanostructures of CuO with graphene.[275] The composites exhibited a durable lifetime with reversible capacities as large as 640 mA h g^{-1} (Fig. 12c).[275]

4.5 Electrochromic devices

Nanostructured Cu$_2$O electrochromic based systems, such as smart windows and optical displays, have been studied since the 1990s.[130] It has been found that Cu$_2$O exhibits cathodic electrochromism, being transparent under visible illumination in their oxidized state and almost black when switched to their reduced state in the presence of an electrolyte containing positive ions such as H$^+$, Li$^+$ and Na$^+$.[130,278–281] Generally, it has been found that the electrochromic process corresponds to the conversion of Cu$_2$O (transparent) to CuO (black) in a reversible reduction–oxidation process (redox).[278,281] To date, the best coloration efficiency obtained by Cu$_2$O nanostructures has been up to 37 cm^2 C^{-1}, which is only one-fourth of the best of those made from nanoporous WO$_3$ (141.5 cm^2 C^{-1}).[278,282] Unfortunately, nanostructured Cu$_2$O requires high coloration voltage and shows poor stability,[279] and further work should be carried out to solve such important issues.

4.6 Sensing applications

Cu$_x$O offers great potential for the development of highly sensitive, yet low cost sensors. This includes optical, gas and bio sensors. Photodetectors are important devices that can be used in various applications, including thermal imaging systems, free-space communications, navigator aids and ozone-layer

This journal is © The Royal Society of Chemistry 2014

J. Mater. Chem. C, 2014, **2**, 5247–5270 | **5261**

monitoring.[283,284] Among the semiconductor materials, Cu_xO has proven to be an attractive material for making photodetectors due to its relatively low band gap and remarkable optoelectronic properties.[70,284–287]

Sahoo *et al.* have demonstrated excellent performance of the photodetector based on Cu_2O nanowires.[285] They adopted the metal–semiconductor–metal (MSM) technique for photon sensing under dark and illumination conditions. Fig. 13(a)–(d) illustrated SEM micrographs of four such MSM devices with channel lengths (*i.e.* spacing between the electrodes) of 210, 260, 580 and 720 nm, respectively.[285] They observed that the channel length significantly influenced the photocurrent and the bias dependence of the photo-to-dark-current ratio (Fig. 13(e)–(h)).[285] Liao *et al.* reported the photoconductivity of Cu_2O nanowires measured under dark and blue (488 nm) laser illumination and the conductance of nanowires increased from 0.7 to 4.3 μS under illumination. Remarkably, the photoconductivity response time was less than three seconds with good reversibility and stability.[70] CuO has also been extensively used in photodetector applications under visible and IR illumination (due to its relatively low band gap).[284,286–288] Recent comprehensive reviews on the usage of CuO in photodetection are found elsewhere.[1]

Cu_xO also offers a great possibility for developing highly sensitive semiconductor-based gas sensors. The sensing properties of Cu_xO can be improved by decreasing its size to nanoscale dimensions (comparable to twice of the Debye length) and by adding appropriate dopants.[126,289] Catalytic nanoparticles such as Pd,[290] Pt,[291] Ag[292] and Au[291,293,294] attached to the Cu_xO surface further increase its sensitivity, mainly due to spill-over effects.[289] Cu_xO thin films have been demonstrated to be highly sensitive towards various gas species including C_2H_5OH,[14,126,294–298] CO,[296,299,300] NO_2 (ref. 14 and 300) and H_2S[53,290,301] (Fig. 14).

The ability to tune the shape and dimensions of Cu_xO thereby creating superior chemical and physical properties can be exploited for chemosensors and biosensors. They also show unique surface chemistry, thermal and electrical properties and a high surface-to-volume ratio which enhance the sensitivity and response of electrochemical sensors.[302]

Cu_xO has been used as a working electrode in electrochemical based biosensors including glucose sensors.[303] Most electrochemical glucose sensors involve the use of the enzyme glucose oxidase. However, the greatest drawback of enzymatic sensors is their lack of stability due to the intrinsic nature of enzymes.[304,305] Development of non-enzymatic sensors, using Cu_xO as the working electrode, has been reported.[305–307] Though non-enzymatic sensors are, by design, quite selective, CuO-based glucose sensors have fast response times, possess a high degree of repeatability and are extremely stable.[303]
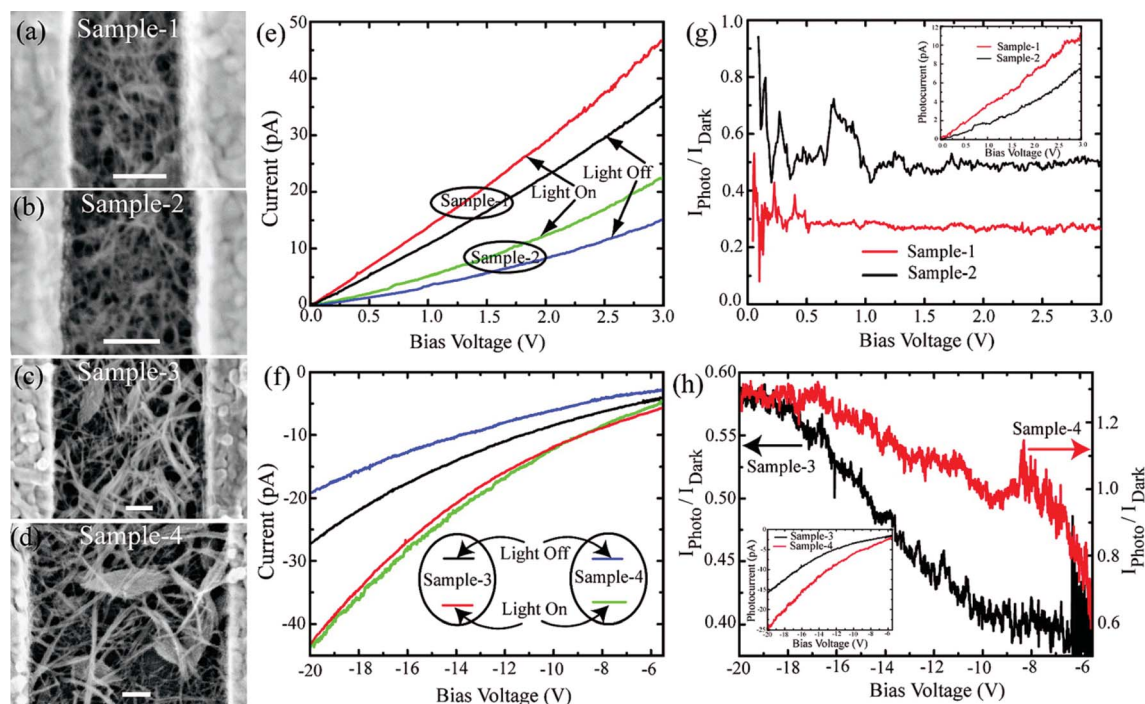
Fig. 13 (a–d) SEM micrographs of Cu_2O nanowire based devices having electrode spacings of 210, 260, 580, and 720 nm, respectively. The electrodes are 3.2 μm wide for all of the devices. The scale bars are 100 nm. The current–voltage (*I–V*) measurements are carried out at dark and under illumination conditions for all four samples. Depending on the interelectrode spacing, the samples are categorized into two sets, set I: sample-1 and sample-2; set II: sample-3 and sample-4. (e and f) *I–V* characteristics of set I and set II, respectively. (g and h) Plot of the ratio of photocurrent (I_{photo}) to the dark current (I_{dark}) *vs.* bias voltage for set I and set II, respectively. Insets of (g) and (h) represent the photocurrent as a function of bias for set I and set II, respectively. Reprinted with permission from (S. Sahoo, S. Husale, B. Colwill, T.-M. Lu, S. Nayak and P. M. Ajayan, *ACS Nano*, 2009, **3**, 3935–3944) copyright (2007) American Chemical Society.
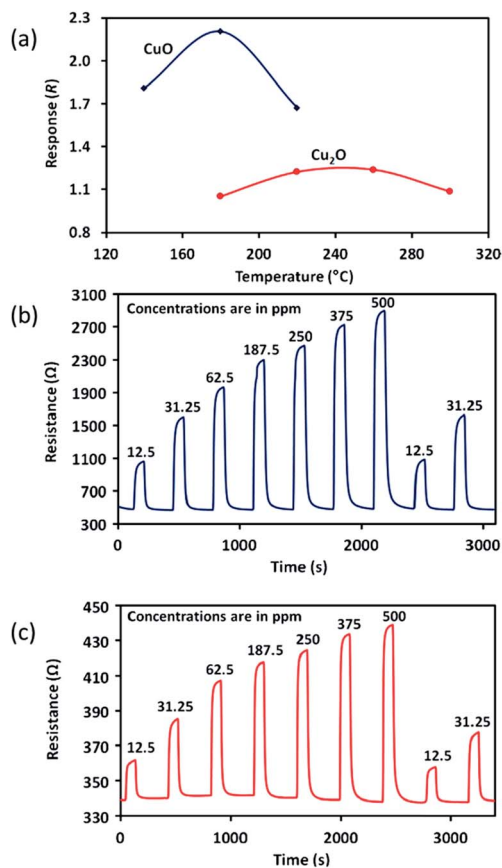
Fig. 14 (a) Sensor response curves of the CuO and Cu$_2$O based sensors towards ethanol (12.5 ppm) at different operating temperatures, dynamic response of (b) CuO based sensors towards ethanol at the optimum operating temperature of 180 °C and (c) Cu$_2$O based sensors towards ethanol at the optimum operating temperature of 260 °C. Reprinted from, A. S. Zoolfakar, M. Z. Ahmad, R. A. Rani, J. Z. Ou, S. Balendhran, S. Zhuiykov, K. Latham, W. Wlodarski and K. Kalantar-zadeh, *Sens. Actuator B Chem.*, **185**, 620–627, copyright (2013) with permission Elsevier.

4.7 Tribology and heat transfer applications

A large number of studies have reported that adding metal oxides such as Cu$_x$O in the form of nanoparticles to lubricants is an effective means to reduce wear and friction.[12,80,308–310] The friction-reduction and anti-wear behaviours are dependent on the characteristics of the nanoparticles including size (mostly in the range of 2–120 nm), morphology and concentration.[12] The colloidal effect, rolling friction effect, third body generation with nanomaterials and protective thin film formation mechanism have been proposed to justify the role of nanomaterials' anti-wear and friction-reduction properties.[80]

Wu *et al.* have compared the tribological properties of two lubricating oils (API-SF engine oil and Base oil) with CuO, TiO$_2$ and diamond nanoparticles used as additives. They found that CuO suspensions showed the highest reduction of the friction coefficient (due to viscosity and rolling effect) and the worn scar depth (owing to reduction of shearing stress) as compared to standard oils without nanoparticles.[12] The shapes of nanoparticles such as spheres, rods, sheets and wires play crucial

roles in tribology in monitoring the friction and anti-wear properties. Recently, Gausian *et al.* have revealed that lubricity enhancement is attributed to the synergistic effect of uninterrupted supplies of CuO nanorods under contact surfaces and their rolling mechanism.[80]

In addition to the enhancement of tribological properties, nanofluids with dispersed Cu$_x$O nanoparticles have great potential for improving heat transfer especially in improving the efficiency of chillers, refrigerators and air-conditioners.[81,310,311] Many studies have reported that mixtures with suspended CuO nanoparticles have higher thermal conductivity than the conventional host fluid.[81] This is due to the thermal conductivity of CuO (76.5 W mK^{-1} which is much higher than ethylene glycol that has a value of 0.26 W mK^{-1}). Lee *et al.* have compared the thermal conductivity of CuO and Al$_2$O$_3$ nanoparticles suspended in ethylene glycol and found that the thermal conductivity of the CuO suspensions is 7% higher than the Al$_2$O$_3$ system.[312]

4.8 Field emission applications

The field emission (FE) properties of Cu$_x$O are far less reported than other oxide materials such as ZnO, SnO$_2$ and In$_2$O$_3$. Due to its relatively narrow band gap, nanostructured Cu$_x$O offers an attractive alternative to serve as a FE emitter.[313–315] In a FE system the emitting capability is believed to be highly dependent on both the properties of the material and configuration of the cathode.[34] It is known that materials with higher aspect ratios and sharp edges generally produce higher FE currents.[55,313,315] Zhu *et al.* have reported FE measurements of CuO nanowire films with a low turn-on field of 3.5–4.5 V μm^{-1}. They obtained a large current density of 0.45 mA cm^{-2} at an applied electric field of 7 V μm^{-1}.[314] Nanostructured Cu$_2$O also exhibits relatively high FE performance. Shi *et al.* have demonstrated Cu$_2$O microporous cubes with a low turn-on field of 3.1 V μm^{-1}. They showed a high current density of 1 mA cm^{-2} at an applied electric field of 11 V μm^{-1}.[55] It has also been reported that Cu$_2$O can be coupled with other metal oxides such as ZnO or TiO$_2$ to enhance its FE performance (Fig. 15).[315–317] This enhanced FE is attributed to the alteration in electron affinity of Cu$_x$O by the other metal oxides forming a nano-heterojunction.[317] Additionally, the presence of the heterojunctions promotes charge separation, where the electrons move to ZnO or TiO$_2$ and the holes move to Cu$_2$O, which reduces the recombination of electron–hole pairs.[317]

4.9 Other applications

Nanostructured Cu$_x$O has also been reported for many applications other than those presented in Sections 4.1 to 4.8. Of note, nanostructured CuO has been used in ceramic resistors[318] and supercapacitors.[319,320] Nanostructured Cu$_2$O has also been incorporated in memristors,[321–323] heterogeneous catalysis,[324–328] anti-fouling[329–331] and thin-film transistors.[2,332,333] Of course, there are other applications for which Cu$_x$O has been used, but these are beyond the scope of this review paper.
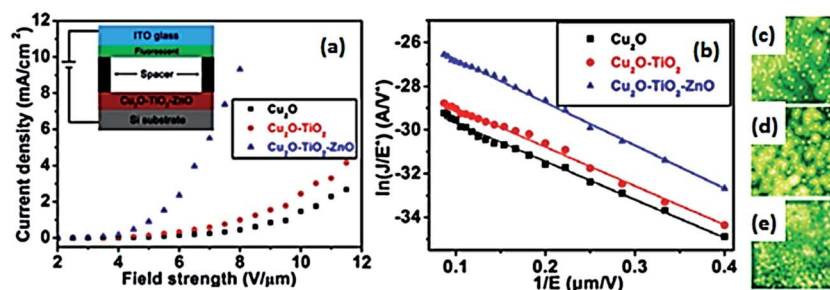
This journal is © The Royal Society of Chemistry 2014

J. Mater. Chem. C, 2014, **2**, 5247–5270 | **5263**

Fig. 15 (a) Field emission $J-E$ curves, (b) corresponding $F-N$ plots of the samples. (c)–(e) Electron emission images of the pure Cu_2O nanopines, Cu_2O-TiO_2-ZnO composite samples, respectively. Reprinted with permission from (Y. Wang, K. Yu, H. H. Yin, C. Q. Song, Z. L. Zhang, S. C. Li, H. Shi, Q. F. Zhang, B. Zhao, Y. F. Zhang and Z. Q. Zhu, *J. Phys. D Appl. Phys.*, 2013, **46**), copyright (2013) by IOP Publishing Ltd.

5. Conclusions and future outlook

In this article, we have presented a comprehensive review of nanostructured Cu_xO focusing on their properties, preparation, processing and device applications. An overview of the material properties, including crystal structures, electronic band structures, optical, vibrational, electrical, thermal and magnetic as well as superconductivity were presented. The effect of doping on the band gap and the enhancement in electrical properties was also detailed. Though much effort has been channeled in producing n-type Cu_xO, the reproducibility and quality issues of the generated films are still questionable. This is potentially due to strong self-compensation effects and dopant solubility issues when n-type dopants are involved. Clearly, these issues must be overcome before high efficiency photovoltaic devices, based on homojunction Cu_2O devices, will be realized.

Numerous synthesis techniques were reviewed, focusing on methods that produce nanostructured Cu_xO. Different synthesis techniques provide flexibility within the constraints of any particular application needs. Therefore, it is essential that exploration of nanostructure Cu_xO synthesis continues and more innovative and low-cost routes are found in order to improve the future of the nanostructured Cu_xO and its many applications.

Additionally, we have discussed the major applications of nanostructured Cu_xO in optics, sensing, tribology, refrigeration, electrochemistry, photocatalysis, high-T_c superconductivity, electrochromics and antimicrobial devices. Due to the versatility of nanostructured Cu_xO, many more applications can be explored and are yet to be investigated.

To date, the majority of work in the area of Cu_xO has been devoted to CuO and Cu_2O, whilst the number of reports on Cu_4O_3 are significantly lower. Despite the fact that there is a very limited number of reports available, the authors believe that the study of nanostructured Cu_4O_3 might provide possible new material insights and unique opportunities for incorporation into a wide-range of applications. Like other copper oxides, nanostructured Cu_4O_3 has the potential to be used in tribology and heat transfer applications as well as antimicrobial devices. As with the other copper oxide structures, the potential gains from developing a low-cost, nanostructured material, like Cu_4O_3 for any of these applications are extremely enticing and expected to be explored.

Notes and references

1 Q. Zhang, K. Zhang, D. Xu, G. Yang, H. Huang, F. Nie, C. Liu and S. Yang, *Prog. Mater. Sci.*, 2014, **60**, 208–337.
2 B. K. Meyer, A. Polity, D. Reppin, M. Becker, P. Hering, P. J. Klar, T. Sander, C. Reindl, J. Benz, M. Eickhoff, C. Heiliger, M. Heinemann, J. Blaesing, A. Krost, S. Shokovets, C. Mueller and C. Ronning, *Phys. Status Solidi B*, 2012, **249**, 1487–1509.
3 K. P. Musselman, A. Marin, L. Schmidt-Mende and J. L. MacManus-Driscoll, *Adv. Funct. Mater.*, 2012, **22**, 2202–2208.
4 V. Gedzevičiūtė, N. Welter, U. Schüssler and C. Weiss, *Archaeol. Anthropol. Sci.*, 2009, **1**, 15–29.
5 P. Colomban, G. Sagon and X. Faurel, *J. Raman Spectrosc.*, 2001, **32**, 351–360.
6 P. E. Russell, *J. Agric. Sci.*, 2005, **143**, 11–25.
7 E. Somers, *J. Sci. Food Agric.*, 1956, **7**, 160–172.
8 I. Omae, *Chem. Rev.*, 2003, **103**, 3431–3448.
9 M. Srinivasan and G. Swain, *Environ. Manage.*, 2007, **39**, 423–441.
10 K. P. Musselman, A. Marin, A. Wisnet, C. Scheu, J. L. MacManus-Driscoll and L. Schmidt-Mende, *Adv. Funct. Mater.*, 2011, **21**, 573–582.
11 O. Akhavan and E. Ghaderi, *Surf. Coat. Technol.*, 2010, **205**, 219–223.
12 Y. Y. Wu, W. C. Tsui and T. C. Liu, *Wear*, 2007, **262**, 819–825.
13 D. Barreca, P. Fornasiero, A. Gasparotto, V. Gombac, C. Maccato, T. Montini and E. Tondello, *ChemSusChem*, 2009, **2**, 230–233.
14 D. D. Li, J. Hu, R. Q. Wu and J. G. Lu, *Nanotechnology*, 2010, **21**, 485502.
15 T. Ito, H. Yamaguchi, K. Okabe and T. Masumi, *J. Mater. Sci.*, 1998, **33**, 3555–3566.
16 W. Y. Ching, Y. N. Xu and K. W. Wong, *Phys. Rev. B: Condens. Matter Mater. Phys.*, 1989, **40**, 7684–7695.
17 S. Sun and Z. Yang, *RSC Adv.*, 2014, **4**, 3804–3822.
18 S. Asbrink and L. J. Norrby, *Acta Crystallogr., Sect. B: Struct. Crystallogr. Cryst. Chem.*, 1970, **26**, 8–15.
19 M. Heinemann, B. Eifert and C. Heiliger, *Phys. Rev. B: Condens. Matter Mater. Phys.*, 2013, **87**, 115111.
20 J. F. Pierson, E. Duverger and O. Banakh, *J. Solid State Chem.*, 2007, **180**, 968–973.

21 M. Okeeffe and J. O. Bovin, *Am. Mineral.*, 1978, **63**, 180–185.

22 C. Frondel, *Am. Mineral.*, 1941, **26**, 657–672.

23 A. E. Rakhshani and F. K. Barakat, *Mater. Lett.*, 1987, **6**, 37–40.

24 M. T. S. Nair, L. Guerrero, O. L. Arenas and P. K. Nair, *Appl. Surf. Sci.*, 1999, **150**, 143–151.

25 M. F. Al-Kuhaili, *Vacuum*, 2008, **82**, 623–629.

26 A. Chen, G. Yang, H. Long, F. Li, Y. Li and P. Lu, *Thin Solid Films*, 2009, **517**, 4277–4280.

27 J. Ghijsen, L. H. Tjeng, J. Vanelp, H. Eskes, J. Westerink, G. A. Sawatzky and M. T. Czyzyk, *Phys. Rev. B: Condens. Matter Mater. Phys.*, 1988, **38**, 11322–11330.

28 A. A. Ogwu, E. Bouquerel, O. Ademosu, S. Moh, E. Crossan and F. Placido, *J. Phys. D: Appl. Phys.*, 2005, **38**, 266–271.

29 M. Izaki, *Thin Solid Films*, 2012, **520**, 2434–2437.

30 K. Nakaoka, J. Ueyama and K. Ogura, *J. Electrochem. Soc.*, 2004, **151**, C661–C665.

31 J. C. Tauc, *Optical Properties of Solids*, North-Holland, Amsterdam, 1972.

32 J. F. Pierson, A. Thobor-Keck and A. Billard, *Appl. Surf. Sci.*, 2003, **210**, 359–367.

33 S. Rehman, A. Mumtaz and S. K. Hasanain, *J. Nanopart. Res.*, 2011, **13**, 2497–2507.

34 H. D. Zheng, J. Z. Ou, M. S. Strano, R. B. Kaner, A. Mitchell and K. Kalantar-Zadeh, *Adv. Funct. Mater.*, 2011, **21**, 2175–2196.

35 A. D. Yoffe, *Adv. Phys.*, 1993, **42**, 173–266.

36 M. Yang and J. He, *J. Colloid Interface Sci.*, 2011, **355**, 15–22.

37 J. Liu, X. Huang, Y. Li, K. M. Sulieman, X. He and F. Sun, *J. Mater. Chem.*, 2006, **16**, 4427–4434.

38 A. Shui, W. Zhu, L. Xu, D. Qin and Y. Wang, *Ceram. Int.*, 2013, **39**, 8715–8722.

39 Y. Gulen, F. Bayansal, B. Sahin, H. A. Cetinkara and H. S. Guder, *Ceram. Int.*, 2013, **39**, 6475–6480.

40 N. M. Basith, J. J. Vijaya, L. J. Kennedy, M. Bououdina and S. Hussain, *J. Nanosci. Nanotechnol.*, 2014, **14**, 2577–2583.

41 N. M. Basith, J. J. Vijaya, L. J. Kennedy and M. Bououdina, *Mater. Sci. Semicond. Process.*, 2014, **17**, 110–118.

42 Y. Peng, Z. Zhang, P. Thien Viet, Y. Zhao, P. Wu and J. Wang, *J. Appl. Phys.*, 2012, **111**.

43 L. Y. Isseroff and E. A. Carter, *Chem. Mater.*, 2013, **25**, 253–265.

44 Y. Chang, J. J. Teo and H. C. Zeng, *Langmuir*, 2005, **21**, 1074–1079.

45 B. Balamurugan and B. R. Mehta, *Thin Solid Films*, 2001, **396**, 90–96.

46 P. Poulopoulos, S. Baskoutas, S. D. Pappas, C. S. Garoufalis, S. A. Droulias, A. Zamani and V. Kapaklis, *J. Phys. Chem. C*, 2011, **115**, 14839–14843.

47 A. Thobor and J. F. Pierson, *Mater. Lett.*, 2003, **57**, 3676–3680.

48 J. F. Pierson, D. Wiederkehr and A. Billard, *Thin Solid Films*, 2005, **478**, 196–205.

49 T. Ito, T. Kawashima, H. Yamaguchi, T. Masumi and S. Adachi, *J. Phys. Soc. Jpn.*, 1998, **67**, 2125–2131.

50 T. Ito, H. Yamaguchi, T. Masumi and S. Adachi, *J. Phys. Soc. Jpn.*, 1998, **67**, 3304–3309.

51 C. Malerba, F. Biccari, C. Leonor Azanza Ricardo, M. D'Incau, P. Scardi and A. Mittiga, *Sol. Energy Mater. Sol. Cells*, 2011, **95**, 2848–2854.

52 K. Borgohain, N. Murase and S. Mahamuni, *J. Appl. Phys.*, 2002, **92**, 1292–1297.

53 J. T. Zhang, J. F. Liu, Q. Peng, X. Wang and Y. D. Li, *Chem. Mater.*, 2006, **18**, 867–871.

54 H.-H. Lin, C.-Y. Wang, H. C. Shih, J.-M. Chen and C.-T. Hsieh, *J. Appl. Phys.*, 2004, **95**, 5889–5895.

55 H. Shi, K. Yu, F. Sun and Z. Zhu, *CrystEngComm*, 2012, **14**, 278–285.

56 H. Shi, K. Yu, Y. Wang, Q. Wang and Z. Zhu, *Appl. Phys. A: Mater. Sci. Process.*, 2012, **108**, 709–717.

57 M. M. Beg and S. M. Shapiro, *Phys. Rev. B: Solid State*, 1976, **13**, 1728–1734.

58 M. Ivanda, D. Waasmaier, A. Endriss, J. Ihringer, A. Kirfel and W. Kiefer, *J. Raman Spectrosc.*, 1997, **28**, 487–493.

59 R. Mittal, S. L. Chaplot, S. K. Mishra and P. P. Bose, *Phys. Rev. B: Condens. Matter Mater. Phys.*, 2007, **75**, 174303.

60 W. Reichardt, F. Gompf, M. Ain and B. M. Wanklyn, *Z. Phys. B: Condens. Matter*, 1990, **81**, 19–24.

61 L. Debbichi, M. C. M. de Lucas, J. F. Pierson and P. Kruger, *J. Phys. Chem. C*, 2012, **116**, 10232–10237.

62 P. H. Shih, C. L. Cheng and S. Y. Wu, *Nanoscale Res. Lett.*, 2013, **8**, 398.

63 R. J. Elliott, *Phys. Rev.*, 1961, **124**, 340–345.

64 Y. K. Jeong and G. M. Choi, *J. Phys. Chem. Solids*, 1996, **57**, 81–84.

65 A. P. Young and C. M. Schwartz, *J. Phys. Chem. Solids*, 1969, **30**, 249–252.

66 S. Suda, S. Fujitsu, K. Koumoto and H. Yanagida, *Jpn. J. Appl. Phys., Part 1*, 1992, **31**, 2488–2491.

67 D. Gopalakrishna, K. Vijayalakshmi and C. Ravidhas, *Ceram. Int.*, 2013, **39**, 7685–7691.

68 Y. Ohya, S. Ito, T. Ban and Y. Takahashi, in *Key Engineering Materials*, eds. N. Murata, K. Shinozaki and T. Kimura, 2000, pp. 113–116.

69 P. Shao, S. Deng, J. Chen, J. Chen and N. Xu, *J. Appl. Phys.*, 2011, **109**, 023710.

70 L. Liao, B. Yan, Y. F. Hao, G. Z. Xing, J. P. Liu, B. C. Zhao, Z. X. Shen, T. Wu, L. Wang, J. T. L. Thong, C. M. Li, W. Huang and T. Yu, *Appl. Phys. Lett.*, 2009, **94**, 113106.

71 Y. W. Tan, X. Y. Xue, Q. Peng, H. Zhao, T. H. Wang and Y. D. Li, *Nano Lett.*, 2007, **7**, 3723–3728.

72 S. Ishizuka and K. Akimoto, *Appl. Phys. Lett.*, 2004, **85**, 4920–4922.

73 K. Mizuno, M. Izaki, K. Murase, T. Shinagawa, M. Chigane, M. Inaba, A. Tasaka and Y. Awakura, *J. Electrochem. Soc.*, 2005, **152**, C179–C182.

74 P. Thien Viet, M. Rao, P. Andreasson, Y. Peng, J. Wang and K. B. Jinesh, *Appl. Phys. Lett.*, 2013, **102**, 032101.

75 D. O. Scanlon and G. W. Watson, *J. Phys. Chem. Lett.*, 2010, **1**, 2582–2585.

76 L. Q. Wang and J. Fan, *Nanoscale Res. Lett.*, 2010, **5**, 1241–1252.

77 X. Wei, H. Zhu, T. Kong and L. Wang, *Int. J. Heat Mass Transfer*, 2009, **52**, 4371–4374.

This journal is © The Royal Society of Chemistry 2014

J. Mater. Chem. C, 2014, **2**, 5247–5270 | 5265

78 Y. J. Hwang, Y. C. Ahn, H. S. Shin, C. G. Lee, G. T. Kim, H. S. Park and J. K. Lee, *Curr. Appl. Phys.*, 2006, **6**, 1068–1071.

79 S. Walia, S. Balendhran, H. Nili, S. Zhuiykov, G. Rosengarten, Q. H. Wang, M. Bhaskaran, S. Sriram, M. S. Strano and K. Kalantar-zadeh, *Prog. Mater. Sci.*, 2013, **58**, 1443–1489.

80 R. Gusain and O. P. Khatri, *J. Mater. Chem. A*, 2013, **1**, 5612–5619.

81 R. Saidur, S. N. Kazi, M. S. Hossain, M. M. Rahman and H. A. Mohammed, *Renewable Sustainable Energy Rev.*, 2011, **15**, 310–323.

82 H. Timm and J. Janek, *Solid State Ionics*, 2005, **176**, 1131–1143.

83 X. Chen, D. Parker, M. H. Du and D. J. Singh, *New J. Phys.*, 2013, **15**, 043029.

84 H. A. Mintsa, G. Roy, C. T. Nguyen and D. Doucet, *Int. J. Therm. Sci.*, 2009, **48**, 363–371.

85 C. H. Li and G. P. Peterson, *J. Appl. Phys.*, 2006, **99**, 084314.

86 M. J. Nine, B. Munkhbayar, M. S. Rahman, H. Chung and H. Jeong, *Mater. Chem. Phys.*, 2013, **141**, 636–642.

87 H. Zhu, D. Han, Z. Meng, D. Wu and C. Zhang, *Nanoscale Res. Lett.*, 2011, **6**, 181.

88 P. A. Korzhavyi, I. L. Soroka, E. I. Isaev, C. Lilja and B. Johansson, *Proc. Natl. Acad. Sci. U. S. A.*, 2012, **109**, 686–689.

89 J. Leitner, D. Sedmidubský, B. Doušová, A. Strejc and M. Nevřiva, *Thermochim. Acta*, 2000, **348**, 49–51.

90 M. W. Chase, C. A. Davies, J. R. Downey, D. J. Frurip, R. A. McDonald and A. N. Syverud, *J. Phys. Chem. Ref. Data*, 1985, **14**, 1–926.

91 E. Gmelin, *Indian J. Pure Appl. Phys.*, 1992, **30**, 596–608.

92 L. V. Gregor, *J. Phys. Chem.*, 1962, **66**, 1645–1647.

93 J. H. Hu and H. L. Johnston, *J. Am. Chem. Soc.*, 1951, **73**, 4550–4551.

94 D. D. Lawrie, J. P. Franck and C.-T. Lin, *Phys. C*, 1998, **297**, 59–63.

95 L. Pinsard-Gaudart, J. Rodriguez-Carvajal, A. Gukasov and P. Monod, *Phys. Rev. B: Condens. Matter Mater. Phys.*, 2004, **69**, 104408.

96 M. H. Whangbo and H. J. Koo, *Inorg. Chem.*, 2002, **41**, 3570–3577.

97 B. X. Yang, J. M. Tranquada and G. Shirane, *Phys. Rev. B: Condens. Matter Mater. Phys.*, 1988, **38**, 174–178.

98 B. X. Yang, J. M. Tranquada and G. Shirane, *Phys. Rev. B: Condens. Matter Mater. Phys.*, 1988, **38**, 174–178.

99 P. J. Brown, T. Chattopadhyay, J. B. Forsyth, V. Nunez and F. Tasset, *J. Phys.: Condens. Matter*, 1991, **3**, 4281–4287.

100 M. S. Seehra and A. Punnoose, *Solid State Commun.*, 2003, **128**, 299–302.

101 X. G. Zheng, T. Mori, K. Nishiyama, W. Higemoto and C. N. Xu, *Solid State Commun.*, 2004, **132**, 493–496.

102 A. Punnoose, H. Magnone, M. S. Seehra and J. Bonevich, *Phys. Rev. B: Condens. Matter Mater. Phys.*, 2001, **64**, 174420.

103 D. Shang, K. Yu, Y. Zhang, J. Xu, J. Wu, Y. e. Xu, L. Li and Z. Zhu, *Appl. Surf. Sci.*, 2009, **255**, 4093–4096.

104 D. Gao, G. Yang, J. Li, J. Zhang, J. Zhang and D. Xue, *J. Phys. Chem. C*, 2010, **114**, 18347–18351.

105 D. Gao, J. Zhang, J. Zhu, J. Qi, Z. Zhang, W. Sui, H. Shi and D. Xue, *Nanoscale Res. Lett.*, 2010, **5**, 769–772.

106 S. H. Pan, J. P. O'Neal, R. L. Badzey, C. Chamon, H. Ding, J. R. Engelbrecht, Z. Wang, H. Eisaki, S. Uchida, A. K. Guptak, K. W. Ng, E. W. Hudson, K. M. Lang and J. C. Davis, *Nature*, 2001, **413**, 282–285.

107 M. A. Kastner, R. J. Birgeneau, G. Shirane and Y. Endoh, *Rev. Mod. Phys.*, 1998, **70**, 897–928.

108 J. M. Tranquada, H. Woo, T. G. Perring, H. Goka, G. D. Gu, G. Xu, M. Fujita and K. Yamada, *Nature*, 2004, **429**, 534–538.

109 M. Karppinen and H. Yamauchi, *Philos. Mag. B*, 1999, **79**, 343–366.

110 H. Yamauchi and M. Karppinen, *Mater. Sci. Eng., B*, 1998, **54**, 92–97.

111 X. Han, K. Han and M. Tao, *Electrochem. Solid-State Lett.*, 2009, **12**, H89–H91.

112 K. Han and M. Tao, in *Photovoltaics for the 21st Century 5*, ed. M. Tao, P. Chang, K. Kakimoto, M. Sunkara, J. Brownson, C. Claeys, K. Rajeshwar and D. Yang, 2010, pp. 103–109.

113 X. Han, K. Han and M. Tao, *Thin Solid Films*, 2010, **518**, 5363–5367.

114 C. A. N. Fernando and S. K. Wetthasinghe, *Sol. Energy Mater. Sol. Cells*, 2000, **63**, 299–308.

115 Y. Okamoto, S. Ishizuka, S. Kato, T. Sakurai, N. Fujiwara, H. Kobayashi and K. Akimoto, *Appl. Phys. Lett.*, 2003, **82**, 1060–1062.

116 B. B. Li, L. Lin, H. L. Shen, F. E. Boafo, Z. F. Chen, B. Liu and R. Zhang, *Eur. Phys. J.: Appl. Phys.*, 2012, **58**, 20303.

117 K. Akimoto, S. Ishizuka, M. Yanagita, Y. Nawa, G. K. Paul and T. Sakurai, *Sol. Energy*, 2006, **80**, 715–722.

118 S. Ishizuka, S. Kato, Y. Okamoto and K. Akimoto, *Appl. Phys. Lett.*, 2002, **80**, 950–952.

119 S. Ishizuka, S. Kato, Y. Okamoto and K. Akimoto, *J. Cryst. Growth*, 2002, **237–239**(part 1), 616–620.

120 C. L. Chu, H. C. Lu, C. Y. Lo, C. Y. Lai and Y. H. Wang, *Phys. B*, 2009, **404**, 4831–4834.

121 H.-C. Lu, C.-L. Chu, C.-Y. Lai and Y.-H. Wang, *Thin Solid Films*, 2009, **517**, 4408–4412.

122 A. S. Reddy, H.-H. Park, V. S. Reddy, K. V. S. Reddy, N. S. Sarma, S. Kaleemulla, S. Uthanna and P. S. Reddy, *Mater. Chem. Phys.*, 2008, **110**, 397–401.

123 H. Zhu, J. Zhang, C. Li, F. Pan, T. Wang and B. Huang, *Thin Solid Films*, 2009, **517**, 5700–5704.

124 A. R. Rastkar, A. R. Niknam and B. Shokri, *Thin Solid Films*, 2009, **517**, 5464–5467.

125 N. G. Elfadill, M. R. Hashim, K. M. Chahrour, M. A. Qaeed and C. Wang, *J. Mater. Sci.: Mater. Electron.*, 2014, **25**, 262–266.

126 A. S. Zoolfakar, M. Z. Ahmad, R. A. Rani, J. Z. Ou, S. Balendhran, S. Zhuiykov, K. Latham, W. Wlodarski and K. Kalantar-zadeh, *Sens. Actuators, B*, 2013, **185**, 620–627.

127 K. J. Blobaum, D. Van Heerden, A. J. Wagner, D. H. Fairbrother and T. P. Weihs, *J. Mater. Res.*, 2003, **18**, 1535–1542.

5266 | *J. Mater. Chem. C*, 2014, **2**, 5247–5270

This journal is © The Royal Society of Chemistry 2014

128 A. V. Richthofen, R. Domnick and R. Cremer, *Fresenius' J. Anal. Chem.*, 1997, **358**, 312–315.

129 P. K. Ooi, S. S. Ng, M. J. Abdullah, H. Abu Hassan and Z. Hassan, *Mater. Chem. Phys.*, 2013, **140**, 243–248.

130 N. Özer and F. Tepehan, *Sol. Energy Mater. Sol. Cells*, 1993, **30**, 13–26.

131 K. Santra, C. K. Sarkar, M. K. Mukherjee and B. Ghosh, *Thin Solid Films*, 1992, **213**, 226–229.

132 B. Balamurugan, B. R. Mehta, D. K. Avasthi, F. Singh, A. K. Arora, M. Rajalakshmi, G. Raghavan, A. K. Tyagi and S. M. Shivaprasad, *J. Appl. Phys.*, 2002, **92**, 3304–3310.

133 V. A. Gevorkyan, A. E. Reymers, M. N. Nersesyan and M. A. Arzakantsyan, *J. Phys.: Conf. Ser.*, 2012, **350**, 012027.

134 S. Kim, K. Hong, K. Kim, I. Lee and J.-L. Lee, *J. Mater. Chem.*, 2012, **22**, 2039–2044.

135 M. Vila, C. Diaz-Guerra and J. Piqueras, *J. Phys. D: Appl. Phys.*, 2010, **43**, 135403.

136 M. Kaur, K. P. Muthe, S. K. Despande, S. Choudhury, J. B. Singh, N. Verma, S. K. Gupta and J. V. Yakhmi, *J. Cryst. Growth*, 2006, **289**, 670–675.

137 A. H. Jayatissa, K. Guo and A. C. Jayasuriya, *Appl. Surf. Sci.*, 2009, **255**, 9474–9479.

138 J. Liang, N. Kishi, T. Soga and T. Jimbo, *Appl. Surf. Sci.*, 2010, **257**, 62–66.

139 Y.-M. Juan, H.-T. Hsueh, T.-C. Cheng, C.-W. Wu and S.-J. Chang, *ECS Solid State Lett.*, 2014, **3**, P30–P32.

140 A. O. Musa, T. Akomolafe and M. J. Carter, *Sol. Energy Mater. Sol. Cells*, 1998, **51**, 305–316.

141 G. Filipic and U. Cvelbar, *Nanotechnology*, 2012, **23**, 194001.

142 Y. Yue, M. Chen, Y. Ju and L. Zhang, *Scr. Mater.*, 2012, **66**, 81–84.

143 L. D. Valladares, D. H. Salinas, A. B. Dominguez, D. A. Najarro, S. I. Khondaker, T. Mitrelias, C. H. W. Barnes, J. A. Aguiar and Y. Majima, *Thin Solid Films*, 2012, **520**, 6368–6374.

144 X. Jiang, T. Herricks and Y. Xia, *Nano Lett.*, 2002, **2**, 1333–1338.

145 L. S. Huang, S. G. Yang, T. Li, B. X. Gu, Y. W. Du, Y. N. Lu and S. Z. Shi, *J. Cryst. Growth*, 2004, **260**, 130–135.

146 F. Mumm and P. Sikorski, *Nanotechnology*, 2011, **22**, 105605.

147 K. L. Zhang, C. Rossi, C. Tenailleau, P. Alphonse and J. Y. Chane-Ching, *Nanotechnology*, 2007, **18**, 275607.

148 Q. Zhang, J. Wang, D. Xu, Z. Wang, X. Li and K. Zhang, *J. Mater. Chem. A*, 2014, **2**, 3865–3874.

149 Q. B. Zhang, D. Xu, T. F. Hung and K. Zhang, *Nanotechnology*, 2013, **24**, 065602.

150 R.-C. Wang and C.-H. Li, *Cryst. Growth Des.*, 2009, **9**, 2229–2234.

151 Q. Zhang, D. Xu, X. Zhou, X. Wu and K. Zhang, *Small*, 2014, **10**, 935–943.

152 H. T. Hsueh, T. J. Hsueh, S. J. Chang, F. Y. Hung, T. Y. Tsai, W. Y. Weng, C. L. Hsu and B. T. Dai, *Sens. Actuators, B*, 2011, **156**, 906–911.

153 Y. Fu, H. Lei, X. Wang, D. Yan, L. Cao, G. Yao, C. Shen, L. Peng, Y. Zhao, Y. Wang and W. Wu, *Appl. Surf. Sci.*, 2013, **273**, 19–23.

154 A. Chen, H. Long, X. Li, Y. Li, G. Yang and P. Lu, *Vacuum*, 2009, **83**, 927–930.

155 M. Kawwam, F. Alharbi, A. Aldwayyan and K. Lebbou, *Appl. Surf. Sci.*, 2012, **258**, 9949–9953.

156 W. Seiler, E. Millon, J. Perrière, R. Benzerga and C. Boulmer-Leborgne, *J. Cryst. Growth*, 2009, **311**, 3352–3358.

157 M. Kawwam, F. H. Alharbi, T. Kayed, A. Aldwayyan, A. Alyamani, N. Tabet and K. Lebbou, *Appl. Surf. Sci.*, 2013, **276**, 7–12.

158 K. P. Muthe, J. C. Vyas, S. N. Narang, D. K. Aswal, S. K. Gupta, D. Bhattacharya, R. Pinto, G. P. Kothiyal and S. C. Sabharwal, *Thin Solid Films*, 1998, **324**, 37–43.

159 K. Kawaguchi, R. Kita, M. Nishiyama and T. Morishita, *J. Cryst. Growth*, 1994, **143**, 221–226.

160 J. Li, Z. Mei, D. Ye, H. Liang, Y. Liu and X. Du, *J. Cryst. Growth*, 2012, **353**, 63–67.

161 D. S. Darvish and H. A. Atwater, *J. Cryst. Growth*, 2011, **319**, 39–43.

162 J. Medina-Valtierra, C. Frausto-Reyes, G. Camarillo-Martinez and J. A. Ramirez-Ortiz, *Appl. Catal., A*, 2009, **356**, 36–42.

163 J. Ramirez-Ortiza, T. Ogura, J. Medina-Valtierra, S. E. Acosta-Ortiz, P. Bosch, J. A. de los Reyes and V. H. Lara, *Appl. Surf. Sci.*, 2001, **174**, 177–184.

164 C. R. Crick and I. P. Parkin, *J. Mater. Chem.*, 2011, **21**, 14712–14716.

165 T. Kosugi and S. Kaneko, *J. Am. Ceram. Soc.*, 1998, **81**, 3117–3124.

166 J. Morales, L. Sanchez, F. Martin, J. R. Ramos-Barrado and M. Sanchez, *Electrochim. Acta*, 2004, **49**, 4589–4597.

167 G. Q. Jian, L. Liu and M. R. Zachariah, *Adv. Funct. Mater.*, 2013, **23**, 1341–1346.

168 T. Ghodselahi, M. A. Vesaghi, A. Shafiekhani, A. Baghizadeh and M. Lameii, *Appl. Surf. Sci.*, 2008, **255**, 2730–2734.

169 D. Barreca, A. Gasparotto, C. Maccato, E. Tondello, O. I. Lebedev and G. Van Tendeloo, *Cryst. Growth Des.*, 2009, **9**, 2470–2480.

170 F. Pola-Albores, W. Antunez-Flores, P. Amezaga-Madrid, E. Rios-Valdovinos, M. Valenzuela-Zapata, F. Paraguay-Delgado and M. Miki-Yoshida, *J. Cryst. Growth*, 2012, **351**, 77–82.

171 P. Pattanasattayavong, S. Thomas, G. Adamopoulos, M. A. McLachlan and T. D. Anthopoulos, *Appl. Phys. Lett.*, 2013, **102**, 163505.

172 O. Waser, M. Hess, A. Guentner, P. Novak and S. E. Pratsinis, *J. Power Sources*, 2013, **241**, 415–422.

173 A. S. Zoolfakar, R. A. Rani, A. J. Morfa, S. Balendhran, A. P. O'Mullane, S. Zhuiykov and K. Kalantar-zadeh, *J. Mater. Chem.*, 2012, **22**, 21767–21775.

174 M. Izaki, M. Nagai, K. Maeda, F. B. Mohamad, K. Motomura, J. Sasano, T. Shinagawa and S. Watase, *J. Electrochem. Soc.*, 2011, **158**, D578–D584.

175 M. Izaki, T. Shinagawa, K.-T. Mizuno, Y. Ida, M. Inaba and A. Tasaka, *J. Phys. D: Appl. Phys.*, 2007, **40**, 3326–3329.

This journal is © The Royal Society of Chemistry 2014

J. Mater. Chem. C, 2014, **2**, 5247–5270 | **5267**

176 J. Sasano, K. Motomura, M. Nagai, F. B. Mohamad and M. Izaki, *Electrochemistry*, 2011, **79**, 831–837.

177 B. M. Fariza, J. Sasano, T. Shinagawa, S. Watase and M. Izaki, *Thin Solid Films*, 2012, **520**, 2261–2264.

178 B. M. Fariza, J. Sasano, T. Shinagawa, H. Nakano, S. Watase and M. Izaki, *J. Electrochem. Soc.*, 2011, **158**, 621–625.

179 J. B. Cui and U. J. Gibson, *J. Phys. Chem. B*, 2010, **114**, 6408–6412.

180 H. Wei, H. Gong, Y. Wang, X. Hu, L. Chen, H. Xu, P. Liu and B. Cao, *CrystEngComm*, 2011, **13**, 6065–6070.

181 P. Poizot, C. J. Hung, M. P. Nikiforov, E. W. Bohannan and J. A. Switzer, *Electrochem. Solid-State Lett.*, 2003, **6**, C21–C25.

182 W. Y. Zhao, W. Y. Fu, H. B. Yang, C. J. Tian, M. H. Li, Y. X. Li, L. N. Zhang, Y. M. Sui, X. M. Zhou, H. Chen and G. T. Zou, *CrystEngComm*, 2011, **13**, 2871–2877.

183 M. Xu, F. Wang, B. Ding, X. Song and J. Fang, *RSC Adv.*, 2012, **2**, 2240–2243.

184 G. Q. Yuan, H. F. Jiang, C. Lin and S. J. Liao, *J. Cryst. Growth*, 2007, **303**, 400–406.

185 G. Yu, X. Hu, D. Liu, D. Sun, J. Li, H. Zhang, H. Liu and J. Wang, *J. Electroanal. Chem.*, 2010, **638**, 225–230.

186 H. Ju, J. K. Lee, J. Lee and J. Lee, *Curr. Appl. Phys.*, 2012, **12**, 60–64.

187 S. Bijani, R. Schrebler, E. A. Dalchiele, M. Gabas, L. Martinez and J. R. Ramos-Barrado, *J. Phys. Chem. C*, 2011, **115**, 21373–21382.

188 M. J. Siegfried and K.-S. Choi, *J. Am. Chem. Soc.*, 2006, **128**, 10356–10357.

189 M. J. Siegfried and K. S. Choi, *Angew. Chem., Int. Ed.*, 2005, **44**, 3218–3223.

190 S. Z. Li, H. Zhang, Y. J. Ji and D. R. Yang, *Nanotechnology*, 2004, **15**, 1428–1432.

191 X. Wang, G. Xi, S. Xiong, Y. Liu, B. Xi, W. Yu and Y. Qian, *Cryst. Growth Des.*, 2007, **7**, 930–934.

192 M. H. Cao, C. W. Hu, Y. H. Wang, Y. H. Guo, C. X. Guo and E. B. Wang, *Chem. Commun.*, 2003, 1884–1885.

193 C. Yang, X. Su, F. Xiao, J. Jian and J. Wang, *Sens. Actuators, B*, 2011, **158**, 299–303.

194 Z. H. Yang, J. Xu, W. X. Zhang, A. P. Liu and S. P. Tang, *J. Solid State Chem.*, 2007, **180**, 1390–1396.

195 L. Liu, K. Hong, T. Hu and M. Xu, *J. Alloys Compd.*, 2012, **511**, 195–197.

196 H. Yu, J. Yu, S. Liu and S. Mann, *Chem. Mater.*, 2007, **19**, 4327–4334.

197 Z. Z. Chen, E. W. Shi, Y. Q. Zheng, W. J. Li, B. Xiao and J. Y. Zhuang, *J. Cryst. Growth*, 2003, **249**, 294–300.

198 S. M. Gupta and M. Tripathi, *Cent. Eur. J. Chem.*, 2012, **10**, 279–294.

199 M. Rajamathi and R. Seshadri, *Curr. Opin. Solid State Mater. Sci.*, 2002, **6**, 337–345.

200 G.-D. Yao, Z.-B. Huo and F.-M. Jin, *Res. Chem. Intermed.*, 2011, **37**, 351–358.

201 L. Zhao, H. Chen, Y. Wang, H. Che, P. Gunawan, Z. Zhong, H. Li and F. Su, *Chem. Mater.*, 2012, **24**, 1136–1142.

202 A. Aslani and V. Oroojpour, *Phys. B*, 2011, **406**, 144–149.

203 A. Aslani, *Phys. B*, 2011, **406**, 150–154.

204 X.-Y. Yu, R.-X. Xu, C. Gao, T. Luo, Y. Jia, J.-H. Liu and X.-J. Huang, *ACS Appl. Mater. Interfaces*, 2012, **4**, 1954–1962.

205 S. J. Chen, X. T. Chen, Z. L. Xue, L. H. Li and X. Z. You, *J. Cryst. Growth*, 2002, **246**, 169–175.

206 J. W. Zhu, D. Li, H. Q. Chen, X. J. Yang, L. Lu and X. Wang, *Mater. Lett.*, 2004, **58**, 3324–3327.

207 R. Wu, Z. Ma, Z. Gu and Y. Yang, *J. Alloys Compd.*, 2010, **504**, 45–49.

208 C. H. Lu, L. M. Qi, J. H. Yang, D. Y. Zhang, N. Z. Wu and J. M. Ma, *J. Phys. Chem. B*, 2004, **108**, 17825–17831.

209 W. Wang, L. Wang, H. Shi and Y. Liang, *CrystEngComm*, 2012, **14**, 5914–5922.

210 K. Chen and D. Xue, *J. Phys. Chem. C*, 2013, **117**, 22576–22583.

211 Z. Yang, J. Xu, W. Zhang, A. Liu and S. Tang, *J. Solid State Chem.*, 2007, **180**, 1390–1396.

212 J. Huang, Y. Dai, C. Gu, Y. Sun and J. Liu, *J. Alloys Compd.*, 2013, **575**, 115–122.

213 H. Zhang, J. Feng and M. Zhang, *Mater. Res. Bull.*, 2008, **43**, 3221–3226.

214 C. Xia, X. Cai, W. Ning and G. Lin, *Anal. Chim. Acta*, 2011, **691**, 43–47.

215 L. Zheng and X. Liu, *Mater. Lett.*, 2007, **61**, 2222–2226.

216 Y. Xu, D. Chen, M. Jiao and K. Xue, *Mater. Res. Bull.*, 2007, **42**, 1723–1731.

217 L. F. Gou and C. J. Murphy, *Nano Lett.*, 2003, **3**, 231–234.

218 M. Yin, C. K. Wu, Y. B. Lou, C. Burda, J. T. Koberstein, Y. M. Zhu and S. O'Brien, *J. Am. Chem. Soc.*, 2005, **127**, 9506–9511.

219 L. Gou and C. J. Murphy, *J. Mater. Chem.*, 2004, **14**, 735–738.

220 M. D. Susman, Y. Feldman, A. Vaskevich and I. Rubinstein, *ACS Nano*, 2014, **8**, 162–174.

221 C.-H. Kuo and M. H. Huang, *J. Phys. Chem. C*, 2008, **112**, 18355–18360.

222 J.-Y. Ho and M. H. Huang, *J. Phys. Chem. C*, 2009, **113**, 14159–14164.

223 H. Xu, W. Wang and W. Zhu, *J. Phys. Chem. B*, 2006, **110**, 13829–13834.

224 W. Z. Wang, G. H. Wang, X. S. Wang, Y. J. Zhan, Y. K. Liu and C. L. Zheng, *Adv. Mater.*, 2002, **14**, 67–69.

225 L. Armelao, D. Barreca, M. Bertapelle, G. Bottaro, C. Sada and E. Tondello, *Thin Solid Films*, 2003, **442**, 48–52.

226 S. C. Ray, *Sol. Energy Mater. Sol. Cells*, 2001, **68**, 307–312.

227 C.-T. Hsieh, J.-M. Chen, H.-H. Lin and H.-C. Shih, *Appl. Phys. Lett.*, 2003, **82**, 3316–3318.

228 Y.-k. Su, C.-m. Shen, H.-t. Yang, H.-l. Li and H.-j. Gao, *Trans. Nonferrous Met. Soc. China*, 2007, **17**, 783–786.

229 X. Hong, G. Wang, W. Zhu, X. Shen and Y. Wang, *J. Phys. Chem. C*, 2009, **113**, 14172–14175.

230 H. Wu, D. Lin and W. Pan, *Appl. Phys. Lett.*, 2006, **89**, 133125.

231 S. M. Sze and K. K. Ng, *Physics of Semiconductor Devices*, John Wiley and Sons, New Jersey, 2007.

232 R. P. Wijesundera, *Semicond. Sci. Technol.*, 2010, **25**, 045015.

233 Y. Hames and S. E. San, *Sol. Energy*, 2004, **77**, 291–294.

5268 | *J. Mater. Chem. C*, 2014, **2**, 5247–5270

This journal is © The Royal Society of Chemistry 2014

234 D. Li, C.-J. Chien, S. Deora, P.-C. Chang, E. Moulin and J. G. Lu, *Chem. Phys. Lett.*, 2011, **501**, 446–450.

235 A. R. Zainun, S. Tomoya, U. Mohd Noor, M. Rusop and I. Masaya, *Mater. Lett.*, 2012, **66**, 254–256.

236 M. Wang, L. Sun, Z. Lin, J. Cai, K. Xie and C. Lin, *Energy Environ. Sci.*, 2013, **6**, 1211–1220.

237 T. Minami, Y. Nishi and T. Miyata, *Appl. Phys. Express*, 2013, **6**, 044101.

238 K. P. Musselman, A. Wisnet, D. C. Iza, H. C. Hesse, C. Scheu, J. L. MacManus-Driscoll and L. Schmidt-Mende, *Adv. Mater.*, 2010, **22**, E254–E285.

239 T. Minami, Y. Nishi, T. Miyata and J. Nomoto, *Appl. Phys. Express*, 2011, **4**, 62301.

240 P. Raksa, S. Nilphai, A. Gardchareon and S. Choopun, *Thin Solid Films*, 2009, **517**, 4741–4744.

241 M. H. Kim and Y. U. Kwon, *J. Phys. Chem. C*, 2011, **115**, 23120–23125.

242 R. Sahay, J. Sundaramurthy, P. S. Kumar, V. Thavasi, S. G. Mhaisalkar and S. Ramakrishna, *J. Solid State Chem.*, 2012, **186**, 261–267.

243 S. Anandan, X. G. Wen and S. H. Yang, *Mater. Chem. Phys.*, 2005, **93**, 35–40.

244 H.-S. Koo, D.-T. Wang, Y.-K. Yu, S.-H. Ho, J.-Y. Jhang, M. Chen and M.-F. Tai, *Jpn. J. Appl. Phys.*, 2012, **51**, 10NE18.

245 G. B. Murdoch, M. Greiner, M. G. Helander, Z. B. Wang and Z. H. Lu, *Appl. Phys. Lett.*, 2008, **93**, 083309.

246 W. P. Hu, K. Manabe, T. Furukawa and M. Matsumura, *Appl. Phys. Lett.*, 2002, **80**, 2640–2641.

247 T. Satoh and H. Fujikawa, *Jpn. J. Appl. Phys., Part 1*, 2007, **46**, 1640–1642.

248 Z. Zheng, B. Huang, Z. Wang, M. Guo, X. Qin, X. Zhang, P. Wang and Y. Dai, *J. Phys. Chem. C*, 2009, **113**, 14448–14453.

249 M. Vaseem, A. Umar, Y. B. Hahn, D. H. Kim, K. S. Lee, J. S. Jang and J. S. Lee, *Catal. Commun.*, 2008, **10**, 11–16.

250 S. P. Meshram, P. V. Adhyapak, U. P. Mulik and D. P. Amalnerkar, *Chem. Eng. J.*, 2012, **204–206**, 158–168.

251 H. Xu, G. Zhu, D. Zheng, C. Xi, X. Xu and X. Shen, *J. Colloid Interface Sci.*, 2012, **383**, 75–81.

252 J. Liu, J. Jin, Z. Deng, S.-Z. Huang, Z.-Y. Hu, L. Wang, C. Wang, L.-H. Chen, Y. Li, G. Van Tendeloo and B.-L. Su, *J. Colloid Interface Sci.*, 2012, **384**, 1–9.

253 M.-h. Yao, Y.-g. Tang, L. Zhang, H.-h. Yang and J.-h. Yan, *Trans. Nonferrous Met. Soc. China*, 2010, **20**, 1944–1949.

254 M. Hara, T. Kondo, M. Komoda, S. Ikeda, K. Shinohara, A. Tanaka, J. N. Kondo and K. Domen, *Chem. Commun.*, 1998, 357–358.

255 P. E. de Jongh, D. Vanmaekelbergh and J. J. Kelly, *Chem. Commun.*, 1999, 1069–1070.

256 G. K. Mor, O. K. Varghese, R. H. T. Wilke, S. Sharma, K. Shankar, T. J. Latempa, K. S. Choi and C. A. Grimes, *Nano Lett.*, 2008, **8**, 1906–1911.

257 W. Siripala, A. Ivanovskaya, T. F. Jaramillo, S. H. Baeck and E. W. McFarland, *Sol. Energy Mater. Sol. Cells*, 2003, **77**, 229–237.

258 M. Ni, M. K. H. Leung, D. Y. C. Leung and K. Sumathy, *Renewable Sustainable Energy Rev.*, 2007, **11**, 401–425.

259 N. Strataki, V. Bekiari, D. I. Kondarides and P. Lianos, *Appl. Catal., B*, 2007, **77**, 184–189.

260 J. Bandara, C. P. K. Udawatta and C. S. K. Rajapakse, *Photochem. Photobiol. Sci.*, 2005, **4**, 857–861.

261 S. Song, J. Tu, L. Xu, X. Xu, Z. He, J. Qiu, J. Ni and J. Chen, *Chemosphere*, 2008, **73**, 1401–1406.

262 H. Yang, J. Yan, Z. Lu, X. Cheng and Y. Tang, *J. Alloys Compd.*, 2009, **476**, 715–719.

263 A. Azam, A. S. Ahmed, M. Oves, M. S. Khan and A. Memic, *Int. J. Nanomed.*, 2012, **7**, 3527–3535.

264 N. Ekthammathat, T. Thongtem and S. Thongtem, *Appl. Surf. Sci.*, 2013, **277**, 211–217.

265 M. S. Hassan, T. Amna, O. B. Yang, M. H. El-Newehy, S. S. Al-Deyab and M.-S. Khil, *Colloids Surf., B*, 2012, **97**, 201–206.

266 I. Perelshtein, G. Applerot, N. Perkas, E. Wehrschuetz-Sigl, A. Hasmann, G. Guebitz and A. Gedanken, *Surf. Coat. Technol.*, 2009, **204**, 54–57.

267 G. Ren, D. Hu, E. W. C. Cheng, M. A. Vargas-Reus, P. Reip and R. P. Allaker, *Int. J. Antimicrob. Agents*, 2009, **33**, 587–590.

268 M. Paschoalino, N. C. Guedes, W. Jardim, E. Mieluarski, J. A. Mielczarski, P. Bowen and J. Kiwi, *J. Photochem. Photobiol., A*, 2008, **199**, 105–111.

269 O. Akhavan and E. Ghaderi, *J. Mater. Chem.*, 2011, **21**, 12935–12940.

270 P. Demchick and A. L. Koch, *J. Bacteriol.*, 1996, **178**, 768–773.

271 B. Wang, X.-L. Wu, C.-Y. Shu, Y.-G. Guo and C.-R. Wang, *J. Mater. Chem.*, 2010, **20**, 10661–10664.

272 J. Y. Xiang, J. P. Tu, L. Zhang, Y. Zhou, X. L. Wang and S. J. Shi, *J. Power Sources*, 2010, **195**, 313–319.

273 L. Ji, Z. Lin, M. Alcoutlabi and X. Zhang, *Energy Environ. Sci.*, 2011, **4**, 2682–2699.

274 Y. J. Mai, X. L. Wang, J. Y. Xiang, Y. Q. Qiao, D. Zhang, C. D. Gu and J. P. Tu, *Electrochim. Acta*, 2011, **56**, 2306–2311.

275 J. Zhou, L. Ma, H. Song, B. Wu and X. Chen, *Electrochem. Commun.*, 2011, **13**, 1357–1360.

276 J. C. Park, J. Kim, H. Kwon and H. Song, *Adv. Mater.*, 2009, **21**, 803–807.

277 W. Wei, Z. Wang, Z. Liu, Y. Liu, L. He, D. Chen, A. Umar, L. Guo and J. Li, *J. Power Sources*, 2013, **238**, 376–387.

278 R. Neskovska, M. Ristova, J. Velevska and M. Ristov, *Thin Solid Films*, 2007, **515**, 4717–4721.

279 M. Ristova, R. Neskovska and V. Mirčeski, *Sol. Energy Mater. Sol. Cells*, 2007, **91**, 1361–1365.

280 T. J. Richardson, J. L. Slack and M. D. Rubin, *Electrochim. Acta*, 2001, **46**, 2281–2284.

281 O. Akhavan, H. Tohidi and A. Z. Moshfegh, *Thin Solid Films*, 2009, **517**, 6700–6706.

282 J. Z. Ou, S. Balendhran, M. R. Field, D. G. McCulloch, A. S. Zoolfakar, R. A. Rani, S. Zhuiykov, A. P. O'Mullane and K. Kalantar-zadeh, *Nanoscale*, 2012, **4**, 5980–5988.

283 T. Y. Zhai, X. S. Fang, M. Y. Liao, X. J. Xu, H. B. Zeng, B. Yoshio and D. Golberg, *Sensors*, 2009, **9**, 6504–6529.

284 S. B. Wang, C. H. Hsiao, S. J. Chang, K. T. Lam, K. H. Wen, S. C. Hung, S. J. Young and B. R. Huang, *Sens. Actuators, A*, 2011, **171**, 207–211.

This journal is © The Royal Society of Chemistry 2014

J. Mater. Chem. C, 2014, **2**, 5247–5270 | **5269**

285 S. Sahoo, S. Husale, B. Colwill, T.-M. Lu, S. Nayak and P. M. Ajayan, *ACS Nano*, 2009, **3**, 3935–3944.

286 B. J. Hansen, N. Kouklin, G. Lu, I. K. Lin, J. Chen and X. Zhang, *J. Phys. Chem. C*, 2010, **114**, 2440–2447.

287 S. Manna, K. Das and S. K. De, *ACS Appl. Mater. Interfaces*, 2010, **2**, 1536–1542.

288 J. Xu, J.-L. Sun, J. Wei and J. Xu, *Appl. Phys. Lett.*, 2012, **100**, 251113.

289 A. Tricoli, M. Righettoni and A. Teleki, *Angew. Chem., Int. Ed.*, 2010, **49**, 7632–7659.

290 H. Kim, C. Jin, S. Park, S. Kim and C. Lee, *Sens. Actuators, B*, 2012, **161**, 594–599.

291 X. Gou, G. Wang, J. Yang, J. Park and D. Wexler, *J. Mater. Chem.*, 2008, **18**, 965–969.

292 G. X. Zhu, H. Xu, Y. Y. Xiao, Y. J. Liu, A. H. Yuan and X. P. Shen, *ACS Appl. Mater. Interfaces*, 2012, **4**, 744–751.

293 M. Ando, T. Kobayashi and M. Haruta, *Catal. Today*, 1997, **36**, 135–141.

294 X.-W. Liu, F.-Y. Wang, F. Zhen and J.-R. Huang, *RSC Adv.*, 2012, **2**, 7647–7651.

295 H. T. Hsueh, S. J. Chang, F. Y. Hung, W. Y. Weng, C. L. Hsu, T. J. Hsueh, S. S. Lin and B. T. Dai, *J. Electrochem. Soc.*, 2011, **158**, J106–J109.

296 Y. Zhang, X. He, J. Li, H. Zhang and X. Gao, *Sens. Actuators, B*, 2007, **128**, 293–298.

297 H. G. Zhang, Q. S. Zhu, Y. Zhang, Y. Wang, L. Zhao and B. Yu, *Adv. Funct. Mater.*, 2007, **17**, 2766–2771.

298 D. Barreca, E. Comini, A. Gasparotto, C. Maccato, C. Sada, G. Sberveglieri and E. Tondello, *Sens. Actuators, B*, 2009, **141**, 270–275.

299 L. Liao, Z. Zhang, B. Yan, Z. Zheng, Q. L. Bao, T. Wu, C. M. Li, Z. X. Shen, J. X. Zhang, H. Gong, J. C. Li and T. Yu, *Nanotechnology*, 2009, **20**, 085203.

300 Y.-S. Kim, I.-S. Hwang, S.-J. Kim, C.-Y. Lee and J.-H. Lee, *Sens. Actuators, B*, 2008, **135**, 298–303.

301 F. Zhang, A. W. Zhu, Y. P. Luo, Y. Tian, J. H. Yang and Y. Qin, *J. Phys. Chem. C*, 2010, **114**, 19214–19219.

302 T. Asefa, C. T. Duncan and K. K. Sharma, *Analyst*, 2009, **134**, 1980–1990.

303 S. Park, H. Boo and T. D. Chung, *Anal. Chim. Acta*, 2006, **556**, 46–57.

304 Z. J. Zhuang, X. D. Su, H. Y. Yuan, Q. Sun, D. Xiao and M. M. F. Choi, *Analyst*, 2008, **133**, 126–132.

305 L. Zhang, H. Li, Y. H. Ni, J. Li, K. M. Liao and G. C. Zhao, *Electrochem. Commun.*, 2009, **11**, 812–815.

306 C. Batchelor-McAuley, Y. Du, G. G. Wildgoose and R. G. Compton, *Sens. Actuators, B*, 2008, **135**, 230–235.

307 C. Batchelor-McAuley, G. G. Wildgoose, R. G. Compton, L. Shao and M. L. H. Green, *Sens. Actuators, B*, 2008, **132**, 356–360.

308 A. H. Battez, R. Gonzalez, J. L. Viesca, J. E. Fernandez, J. M. D. Fernandez, A. Machado, R. Chou and J. Riba, *Wear*, 2008, **265**, 422–428.

309 T. Oishi, M. Goto, A. Kasahara and M. Tosa, *Surf. Interface Anal.*, 2004, **36**, 1259–1261.

310 M. A. Kedzierski, *Int. J. Refrig.*, 2012, **35**, 1997–2002.

311 S.-s. Bi, L. Shi and L.-l. Zhang, *Appl. Therm. Eng.*, 2008, **28**, 1834–1843.

312 S. Lee, S. U. S. Choi, S. Li and J. A. Eastman, *J. Heat Transfer*, 1999, **121**, 280–289.

313 C. T. Hsieh, J. M. Chen, H. H. Lin and H. C. Shih, *Appl. Phys. Lett.*, 2003, **83**, 3383–3385.

314 Y. W. Zhu, T. Yu, F. C. Cheong, X. J. Xui, C. T. Lim, V. B. C. Tan, J. T. L. Thong and C. H. Sow, *Nanotechnology*, 2005, **16**, 88–92.

315 Y. Wang, S. C. Li, H. Shi and K. Yu, *Nanoscale*, 2012, **4**, 7817–7824.

316 R. C. Wang and C. H. Li, *Cryst. Growth Des.*, 2009, **9**, 2229–2234.

317 Y. Wang, K. Yu, H. H. Yin, C. Q. Song, Z. L. Zhang, S. C. Li, H. Shi, Q. F. Zhang, B. Zhao, Y. F. Zhang and Z. Q. Zhu, *J. Phys. D: Appl. Phys.*, 2013, **46**, 175303.

318 S. Tanaka, Y. Sawai and A. Chiba, *J. Eur. Ceram. Soc.*, 2004, **24**, 289–293.

319 K. Krishnamoorthy and S.-J. Kim, *Mater. Res. Bull.*, 2013, **48**, 3136–3139.

320 D. P. Dubal, G. S. Gund, C. D. Lokhande and R. Holze, *Mater. Res. Bull.*, 2013, **48**, 923–928.

321 B. Singh, B. R. Mehta, D. Varandani, A. V. Savu and J. Brugger, *Nanotechnology*, 2012, **23**, 495707.

322 A. Chen, S. Haddad, Y. C. Wu, Z. Lan, T. N. Fang and S. Kaza, *Appl. Phys. Lett.*, 2007, **91**, 123517.

323 W.-Y. Yang, W.-G. Kim and S.-W. Rhee, *Thin Solid Films*, 2008, **517**, 967–971.

324 I. Najdovski, P. Selvakannan, S. K. Bhargava and A. P. O'Mullane, *Nanoscale*, 2012, **4**, 6298–6306.

325 J. B. Reitz and E. I. Solomon, *J. Am. Chem. Soc.*, 1998, **120**, 11467–11478.

326 S. Song, R. Rao, H. Yang and A. Zhang, *J. Phys. Chem. C*, 2010, **114**, 13998–14003.

327 Y. Xu, H. Wang, Y. Yu, L. Tian, W. Zhao and B. Zhang, *J. Phys. Chem. C*, 2011, **115**, 15288–15296.

328 R. Prucek, L. Kvitek, A. Panacek, L. Vancurova, J. Soukupova, D. Jancik and R. Zboril, *J. Mater. Chem.*, 2009, **19**, 8463–8469.

329 S. Zhuiykov, E. Kats, D. Marney and K. Kalantar-zadeh, *Prog. Org. Coat.*, 2011, **70**, 67–73.

330 S. Zhuiykov and K. Kalantar-zadeh, *Electrochim. Acta*, 2012, **73**, 105–111.

331 S. Zhuiykov, D. Marney, E. Kats and K. Kalantar-Zadeh, *Sens. Actuators, B*, 2011, **153**, 312–320.

332 E. Fortunato, V. Figueiredo, P. Barquinha, E. Elamurugu, R. Barros, G. Goncalves, S.-H. K. Park, C.-S. Hwang and R. Martins, *Appl. Phys. Lett.*, 2010, **96**, 192102.

333 X. Zou, G. Fang, L. Yuan, M. Li, W. Guan and X. Zhao, *IEEE Electron Device Lett.*, 2010, **31**, 827–829.

5270 | *J. Mater. Chem. C*, 2014, **2**, 5247–5270

This journal is © The Royal Society of Chemistry 2014